

Numerical behavior of the Keplerian Integral methods for initial orbit determination

Óscar Rodríguez ¹, Giovanni F. Gronchi ¹, Giulio Baù ¹, and Robert Jedicke ²

¹Dipartimento di Matematica, Università di Pisa, Italy

²Institute for Astronomy, University of Hawai'i, USA

January 3, 2024

Abstract

We investigate the behaviour of two recent methods for the computation of preliminary orbits. These methods are based on the conservation laws of Kepler's problem, and enable the linkage of very short arcs of optical observations even when they are separated in time by a few years. Our analysis is performed using both synthetic and real data of 822 main belt asteroids. The differences between computed and true orbital elements have been analysed for the true linkages, as well as the occurrence of alternative solutions. Some metrics have been introduced to quantify the results, with the aim of discarding as many of the false linkages as possible and keeping the vast majority of true ones. These numerical experiments provide thresholds for the metrics which take advantage of the knowledge of the *ground truth*: the values of these thresholds can be used in normal operation mode, when we do not know the correct values of the orbital elements and whether the linkages are true or false.

1 Introduction

Modern asteroid surveys, like Pan-STARRS [5] and Catalina [4], collect a large number of optical observations that are grouped in *very short arcs* (VSA), also called *tracklets*. The information contained in a VSA is usually not sufficient to compute a reliable least squares orbit with classical methods [15, 14, 7]. In this case, we can try to compute an orbit by combining the data from two or more VSAs under the assumption that they belong to the same celestial body. This operation is called *linkage*, see Milani and Gronchi [16, Chap. 7].

Among the existing linkage algorithms, here we consider the so-called Keplerian integrals (KI) methods. These methods provide a polynomial equation for the computation of a preliminary orbit from the conservation laws of Kepler's dynamics, i.e. angular momentum, the Laplace-Lenz vector and energy. The conservation of angular momentum and energy were already used for this problem in [22, 21], however the authors did not fully exploit the algebraic character of the resulting equations. More recently, in a series of papers [11, 12, 9] derived from the Keplerian conservation laws polynomial equations of degree 48, 20 and 9, respectively, for the linkage of two VSAs. In [10] the authors showed that the polynomial of degree 9 introduced in [9] is optimal in some sense, and derived an equation of degree 8 for the linkage of three VSAs.

In this work we analyse the numerical behaviour of two KI methods, here denoted by `link2` and `link3`. The first method, introduced in [9], uses two VSAs and a suitable combination of all the conserved quantities. The second, presented in [10], employs three VSAs and the conservation of the angular momentum only. These algorithms allow for a fast computation of orbits, but their sensitivity to astrometric errors has not yet been systematically analysed. Understanding the performance of these methods is crucial when working with large databases of VSAs such as the isolated tracklet file (ITF)¹ which is available from the Minor Planet Center (MPC). The ITF is an ever changing list of unlinked tracklets, mainly provided by Pan-STARRS1 and Catalina, with more than 4 and 2 million observations, respectively. However, there are also observations from many other telescopes, thus the quality of the data in the ITF is heterogeneous. For this reason, we study the sensitivity of `link2` and `link3` to different levels of astrometric errors. During the last years some effort has been made to compute orbits with the ITF data [18, 13, 23] and the size of this file has been considerably reduced. [13] used a tracklet clustering technique to define an algorithm with complexity $\mathcal{O}(N \log N)$, where N is the total number of tracklets. [18] employed an identification algorithm of attribution type that took into account the higher apparent rates of motion of NEAs.

From the results of our study, we think that the KI methods can be efficient tools for initial orbit determination, complementary to the existing ones. In fact, as opposite to the other algorithms, they are able to link tracklets that are separated in time even by a few years.

The structure of this paper is the following. In Section 2 we present the `link2` and `link3` methods and the indicators that we use to analyse the quality of the solutions. In Section 3 we explain the generation of the test data sets. Section 4 is devoted to the analysis of the numerical behaviour of `link2` and `link3` when applied to synthetic data. In Section 5 we apply the two KI methods to real data and we compare their performance to that obtained in Section 4. Finally, in Section 6 we estimate the efficiency of `link2` in producing correct linkages under simplistic assumptions: in particular, we estimate the number of sets of 4 tracklets (correctly or incorrectly associated) that need to be examined as a function of the probability of identifying correct associations.

2 The KI methods

Let us consider a set of $m \geq 2$ optical observations of a celestial body $\{(\alpha_i, \delta_i) \mid i = 1, \dots, m\}$, where α_i, δ_i are right ascension and declination at epochs t_i , $i = 1, \dots, m$, that are close in time to each other. From these data we can compute the *attributable* vector

$$\mathcal{A} = (\alpha, \delta, \dot{\alpha}, \dot{\delta}),$$

representing the angular position and angular rate of the body at the mean time $\bar{t} = \frac{1}{m} \sum_{i=1}^m t_i$. We denote by \mathbf{r} and \mathbf{q} the heliocentric positions of the asteroid and the observer at time \bar{t} . In this way, the topocentric position of the asteroid is given by $\boldsymbol{\rho} = \mathbf{r} - \mathbf{q}$. Setting $\rho = |\boldsymbol{\rho}|$, we can write $\boldsymbol{\rho} = \rho \mathbf{e}^\rho$, where

$$\mathbf{e}^\rho = (\cos \alpha \cos \delta, \sin \alpha \cos \delta, \sin \delta),$$

is a known vector, the *line of sight*.

The Keplerian integrals (KI) methods exploit the conservation laws of Kepler's dynamics for the

¹<http://www.minorplanetcenter.net/iau/ITF/itf.txt.gz>

linkage. The conserved quantities are

$$\mathbf{c} = \mathbf{r} \times \dot{\mathbf{r}}, \quad \mathcal{E} = \frac{1}{2}|\dot{\mathbf{r}}|^2 - \frac{\mu}{|\mathbf{r}|}, \quad \mathbf{L} = \frac{1}{\mu}\dot{\mathbf{r}} \times \mathbf{c} - \frac{\mathbf{r}}{|\mathbf{r}|}, \quad (1)$$

which correspond to the angular momentum, energy, and Laplace-Lenz vector of the orbit, respectively.

Given an attributable \mathcal{A} at the epoch \bar{t} , the quantities (1) can be written as algebraic functions of the unknowns $\rho, \dot{\rho}$, with coefficients depending on the attributable \mathcal{A} and on the heliocentric position \mathbf{q} and velocity $\dot{\mathbf{q}}$ of the observer.

2.1 The link2 algorithm

We briefly recall the algorithm introduced in [9] for the linkage of two VSAs. Given two attributables of the same object $\mathcal{A}_1, \mathcal{A}_2$ at the epochs \bar{t}_1, \bar{t}_2 , we consider the system

$$\mathbf{c}_1 = \mathbf{c}_2, \quad [\mu(\mathbf{L}_1 - \mathbf{L}_2) - (\mathcal{E}_1 \mathbf{r}_1 - \mathcal{E}_2 \mathbf{r}_2)] \times (\mathbf{r}_1 - \mathbf{r}_2) = \mathbf{0}, \quad (2)$$

where the subscripts refer to the two epochs and we assume 2-body Keplerian motion between the two times. System (2) is polynomial, is composed of 6 equations in 4 unknowns $(\rho_1, \rho_2, \dot{\rho}_1, \dot{\rho}_2)$, and is therefore over-determined. Nevertheless, we can show that this system is consistent, i.e. it always has solutions, at least in the complex field, even when the two tracklets belong to different objects.

By elimination of variables, system (2) leads to a polynomial equation of degree 9 in one of the two unknown topocentric ranges $(\rho_1$ or $\rho_2)$.

From the positive roots of this polynomial we obtain quadruples of solutions of (2). These correspond to pairs of Keplerian orbits at epochs \tilde{t}_1, \tilde{t}_2 , obtained by applying aberration correction to \bar{t}_1, \bar{t}_2 .

2.1.1 The χ_4 norm

The preliminary orbits computed with the `link2` algorithm have an associated covariance matrix. Consider a preliminary orbit at epoch \tilde{t}_1 . This orbit and its covariance are propagated to the epoch \bar{t}_2 of the second attributable \mathcal{A}_2 , with covariance matrix Γ_2 . Then, we can compute a propagated attributable \mathcal{A}_p , with marginal covariance matrix Γ_p , see [16, Chap.7], [17]. We quantify the difference between the two attributables \mathcal{A}_p and \mathcal{A}_2 by the χ_4 norm,

$$\chi_4 = \sqrt{(\mathcal{A}_p - \mathcal{A}_2) \cdot [C_2 - C_2 \Gamma_0 C_2] (\mathcal{A}_p - \mathcal{A}_2)^t}, \quad (3)$$

where

$$C_2 = \Gamma_2^{-1}, \quad \Gamma_0 = C_0^{-1},$$

with

$$C_0 = C_2 + C_p, \quad C_p = \Gamma_p^{-1}.$$

We will show that the χ_4 norm can be used to select good solutions from `link2` using a threshold for the acceptable solutions.

2.2 The link3 algorithm

Given three attributables $\mathcal{A}_1, \mathcal{A}_2, \mathcal{A}_3$ of an asteroid, one or more preliminary orbits can be computed by imposing the conservation of the angular momentum only:

$$\mathbf{c}_1 = \mathbf{c}_2, \quad \mathbf{c}_2 = \mathbf{c}_3. \quad (4)$$

System (4) gives us 6 scalar equations in the 6 unknowns $\rho_1, \dot{\rho}_1, \rho_2, \dot{\rho}_2, \rho_3, \dot{\rho}_3$. Let us define

$$\mathbf{D} = \mathbf{q} \times \mathbf{e}^\rho.$$

If relation

$$\mathbf{D}_1 \times \mathbf{D}_2 \cdot \mathbf{D}_3 \neq 0,$$

holds, then equations (4) are equivalent to

$$\begin{aligned} 0 &= (\mathbf{c}_i - \mathbf{c}_j) \cdot \mathbf{D}_i \times \mathbf{D}_j, \\ 0 &= (\mathbf{c}_i - \mathbf{c}_j) \cdot \mathbf{D}_i \times (\mathbf{D}_i \times \mathbf{D}_j), \end{aligned}$$

with $(i, j) = (1, 2), (2, 3), (3, 1)$. By elimination of variables, as explained in [10], we can write a polynomial equation of degree 8 in the ρ_2 unknown only, and then reconstruct the values of the other variables. Note that we can always discard one of the solutions, because it corresponds to a *straight line* solution, with zero angular momentum.

2.2.1 The star norm

The link3 method only imposes the equality of the angular momentum \mathbf{c} at the three different times. Note that, given a Keplerian orbit defined by the orbital elements $(a, e, i, \Omega, \omega, \ell)$, we can express its angular momentum as

$$\mathbf{c} = \sqrt{\mu a(1 - e^2)} (\sin \Omega \sin i, -\cos \Omega \sin i, \cos i),$$

where μ is the gravitational parameter. Therefore, while Ω, i , and $c^2 = \mu a(1 - e^2)$ take the same values at the three epochs, the orbital elements ω, ℓ, a , and e might be different. In light of this consideration, we introduce a norm that accounts for such differences.

Given a triplet of attributables $\mathbf{A} = (\mathcal{A}_1, \mathcal{A}_2, \mathcal{A}_3)$ with covariance matrices $\Gamma_{\mathcal{A}_j}$ we consider the difference

$$\begin{aligned} \Delta_{jk} &= \left(a_j - a_k, (\omega_j - \omega_k + \pi) \pmod{2\pi} - \pi, \right. \\ &\quad \left. (\ell_j - [\ell_k + n(a_j)(\tilde{t}_j - \tilde{t}_k)] + \pi) \pmod{2\pi} - \pi \right), \end{aligned}$$

where $n(a) = \sqrt{\mu/a^3}$ is the mean motion and $j, k \in \{1, 2, 3\}$ refer to the quantities at the three times. We introduce the vector $\mathbf{\Delta} = (\Delta_{12}, \Delta_{32})$ and the matrix

$$\Gamma_{\mathbf{A}} = \begin{pmatrix} \Gamma_{\mathcal{A}_1} & 0 & 0 \\ 0 & \Gamma_{\mathcal{A}_2} & 0 \\ 0 & 0 & \Gamma_{\mathcal{A}_3} \end{pmatrix}.$$

Setting

$$\Gamma_{\Delta} = \frac{\partial \Delta}{\partial \mathbf{A}} \Gamma_{\mathbf{A}} \left[\frac{\partial \Delta}{\partial \mathbf{A}} \right]^t, \quad C_{\Delta} = \Gamma_{\Delta}^{-1},$$

we define the \star norm as

$$\Delta_{\star} = \sqrt{\Delta C_{\Delta} \Delta^t}. \quad (5)$$

More details about the computation of this norm can be found in [10].

2.3 The *rms* norm

Another metric for the quality of preliminary orbits is:

$$rms = \sqrt{\frac{1}{n} \sum_{i=1}^n \left[\Delta_{\alpha_i}^2 \cos^2 \delta_i + \Delta_{\delta_i}^2 \right]}, \quad (6)$$

where $\Delta_{\alpha_i} = \alpha_i - \alpha(\bar{t}_i)$, $\Delta_{\delta_i} = \delta_i - \delta(\bar{t}_i)$ are the residuals of the observations, with $\alpha(\bar{t}_i), \delta(\bar{t}_i)$ coming from a 2-body propagation of the preliminary orbit.

2.4 Least squares norm

After computing a preliminary orbit with `link2` or `link3`, a differential corrections scheme [16, Chap. 5] can be used to determine a least squares orbit.² If this scheme is successful, we can define the following metric:

$$R_{LS} = \sqrt{\frac{1}{n} \sum_{i=1}^n \left[w_i \left(\Delta_{\alpha_i}^2 \cos^2 \delta_i + \Delta_{\delta_i}^2 \right) \right]}, \quad (7)$$

with $\alpha(\bar{t}_i), \delta(\bar{t}_i)$ coming from the full n -body propagation of the least squares orbit. Here we allow different weights w_i for the observations.

Differential corrections are computationally more expensive than the algorithms for the determination of a preliminary orbit, and the iterative process must begin with a ‘good’ orbit close to reality. If the preliminary solution computed with `link2` or `link3` is not good enough then differential corrections will not converge or will converge to a wrong solution.

3 The data sets

We generated our test data sets from real data submitted by Pan-STARRS1 [5] to the MPC over the 8.5 year period from 2011-01-30 through 2019-07-28 inclusive (see Figure 1). This technique ensures that we are using consistent data from a single survey with a real observation cadence within a night and across many years. We restricted the test data to main belt objects because they dominate the statistics of any asteroid survey and extracted triplets of random tracklets corresponding to the same object for 822 asteroids.

²We used the `fdiff_cor` routine of the `OrbFit` package for the differential corrections (<http://adams.dm.unipi.it/orbfit/>).

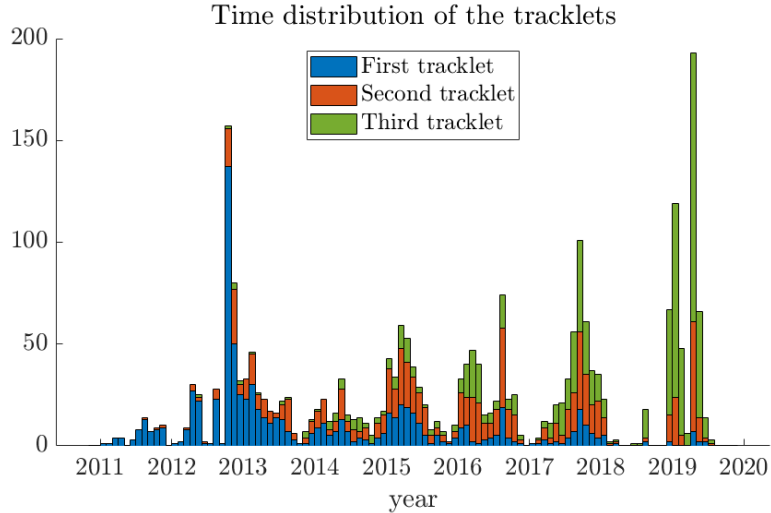


Figure 1: Time distribution of the tracklets in our *matched real* data sample.

We also required that each of the tracklets must have ≥ 3 detections. These observations are our *matched real* data which include all the vagaries of an actual operational survey including the requirements that the observations be acquired at night, when the telescope is operational, when the sky is clear, scheduling issues, etc. The average time between any pair of tracklets corresponding to the same object is about 2.6 years. We selected this data set in order to test the capability of the algorithms to link tracklets with different time separation (see Figure 2).

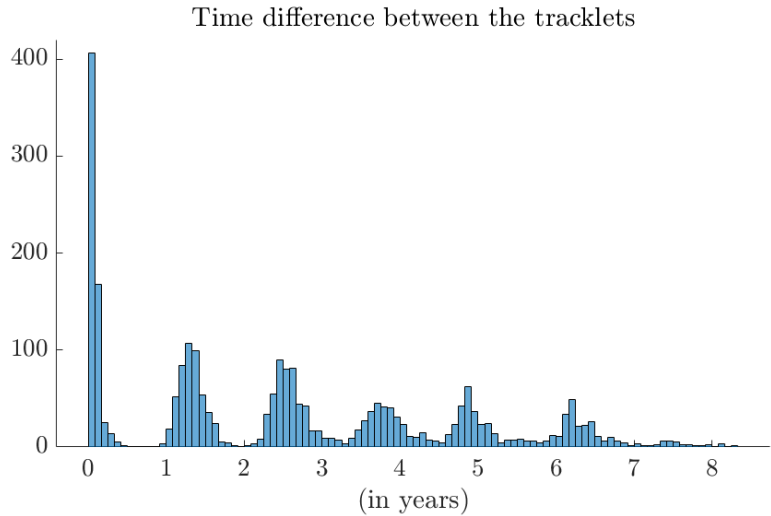


Figure 2: Time difference between pairs of tracklets for the same object.

We then generated synthetic data sets for the same objects using the nominal orbit for each object as reported by the MPC and the actual times of observations from the *matched real* Pan-STARRS1 data. We did so using a simple 2-body calculation and a full n -body integration with all the planets and major asteroids as implemented in OpenOrb [8]. In both the 2-body and n -body cases we generated synthetic data sets in which a random error was introduced into the astrometric observations by generating a random offset from the calculated positions according to a 2d Gaussian with standard deviations (σ) of $0.1''$, $0.2''$, $0.5''$, and $1.0''$.

The synthetic data set with no introduced error allows us to determine our algorithm's performance

on perfect data. The other data sets allow us to characterise how the algorithms’s performance degrades with increasing astrometric error typical of other and historical asteroid surveys with our eventual goal of applying `link2` and `link3` to the MPC’s ITF.

Note that the data sets used for `link2` are obtained from those of `link3` by randomly selecting two tracklets per object from the three available (i.e. 1644 tracklets for each data set), and the same choice is maintained throughout all the numerical tests.

4 Testing the KI methods with synthetic data

In this section we characterise the performance of `link2` and `link3` in terms of their sensitivity to astrometric error.

We first consider the case of *true* linkages, i.e. linkages of tracklets belonging to the same object. In Section 4.4 we shall investigate how many *false* linkages (i.e. linkages of tracklets belonging to different objects) produce solutions.

`link3` is applied to the triplet of tracklets generated for each object while `link2` is applied to two tracklets as explained in Section 3. In this way, we determine the percentage of cases for which we are able to find solutions with each method, and investigate how this percentage evolves as we increase the error in the simulated data. For the moment, we are not concerned with the quality of the solutions.

The percentage of linkages found, out of all the possible true ones, is high with both methods (see Figure 3). `link2` recovers a higher percentage of linkages than `link3`. In particular, it allows us to find more than 86% of the linkages when the astrometric error is large, and more than 95% when the error is small, reaching 100% in the ideal case of observations with no error with both dynamical models (2-body and n -body). `link3` is affected by astrometric error in a more severe way, it identifies only about 70% of the linkages with a large error in the observations, and does not achieve the same high percentages of linkages found by `link2` even when the error is small or null. Most of the linkages recovered with `link2` provide more than one solution. This also occurs with `link3` but the percentage is lower.

A natural question that arises at this point is whether the quality of the solutions obtained is good. To answer this question we investigate the errors in the orbital elements $(a, e, i, \Omega, \omega)$ and in the angular momentum c computed from the output of `link2` and `link3`. In Figure 4 we plot the probability density function (PDF) of the logarithm of the error for each component and for the different data sets. This figure was produced by choosing always the solution with the lowest value of the orbit comparison criterion defined in [20, 6], hereafter simply D . The quality of the solutions is better using `link2` than `link3`. The PDF obtained with `link2` has a single local maximum and, as expected, the performance deteriorates for larger astrometric errors. The computed values of some elements are closer to the true ones than others: the orbital plane (defined by i and Ω) is much better determined than the perihelion position (given by ω). Furthermore, when the error is greater than $0.5''$ the value of ω is completely wrong.

In Figure 4 the PDF often presents two local maxima with `link3`, and the second maximum increases with the astrometric error. In this case we have a large number of false solutions that need to be discarded *a posteriori*. Like `link2`, `link3` determines some orbital elements better than others.

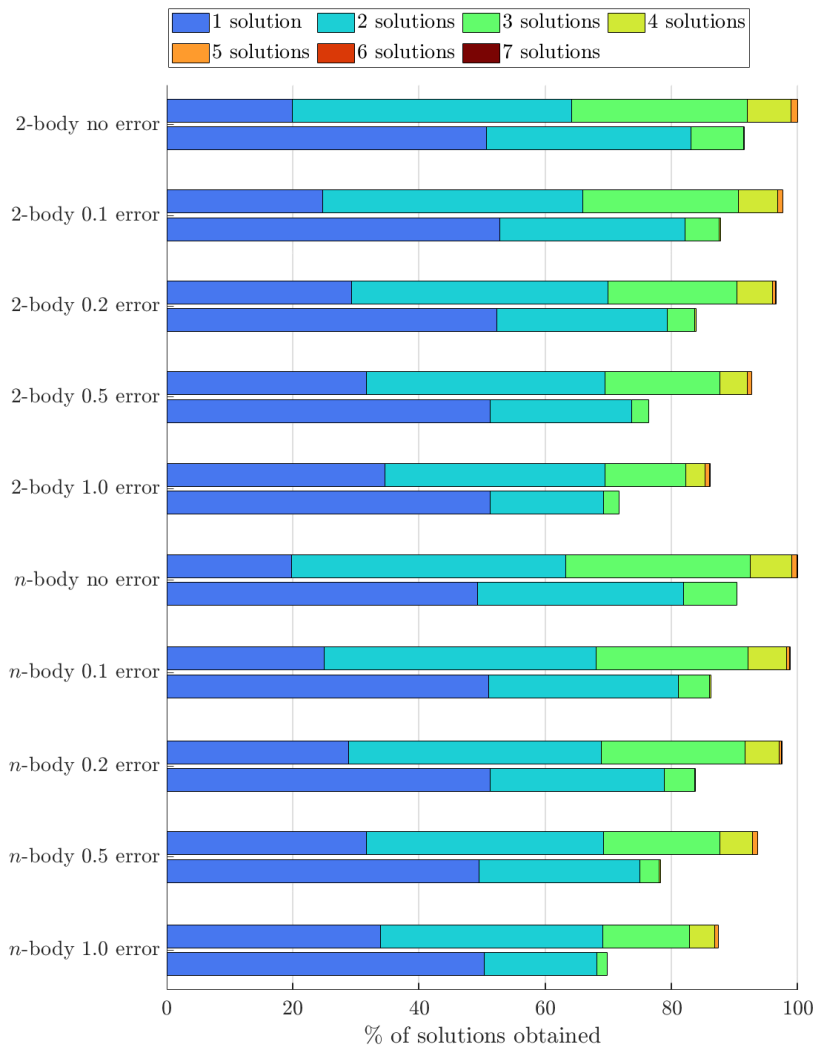


Figure 3: Percentage of linkages and multiplicity of the solutions obtained with `link2` (above) and `link3` (below) for each of the 10 synthetic data sets.

Considering also that `link3` recovers fewer solutions than `link2` (see Figure 3), we conclude that it is preferable to use the latter.

As we have mentioned, both methods often give multiple solutions. Some of them can be discarded using indicators such as the χ_4 with `link2` or the Δ_* with `link3` (see Sections 2.1.1, 2.2.1). These norms will play a crucial role to rule out false linkages. In Figure 5 we see how the percentage of linkages with a different number of accepted solutions changes as the value of the acceptance threshold of the χ_4 increases. We note that by choosing the value of this threshold corresponding to the dark blue peak, we loose only $\approx 10\%$ of the possible linkages and most of the accepted linkages give only one solution. This phenomenon is shown by all data sets, being more evident with a small or zero error (see for example the left plot of Figure 5).

The values of the χ_4 and Δ_* norms are important to evaluate the quality of the solutions (see Figures 6 and 7). It is common to identify two orbits when $D \leq 0.2$, see [20, 19]. In Figure 6 we present the values of the logarithms of D and χ_4 with `link2` for observations generated by an n -body propagation and with different astrometric errors. Note that $\log_{10} 0.2 \approx -0.7$. Here as in most of the next plots, we select the best solution in terms of D in case of linkages with more than

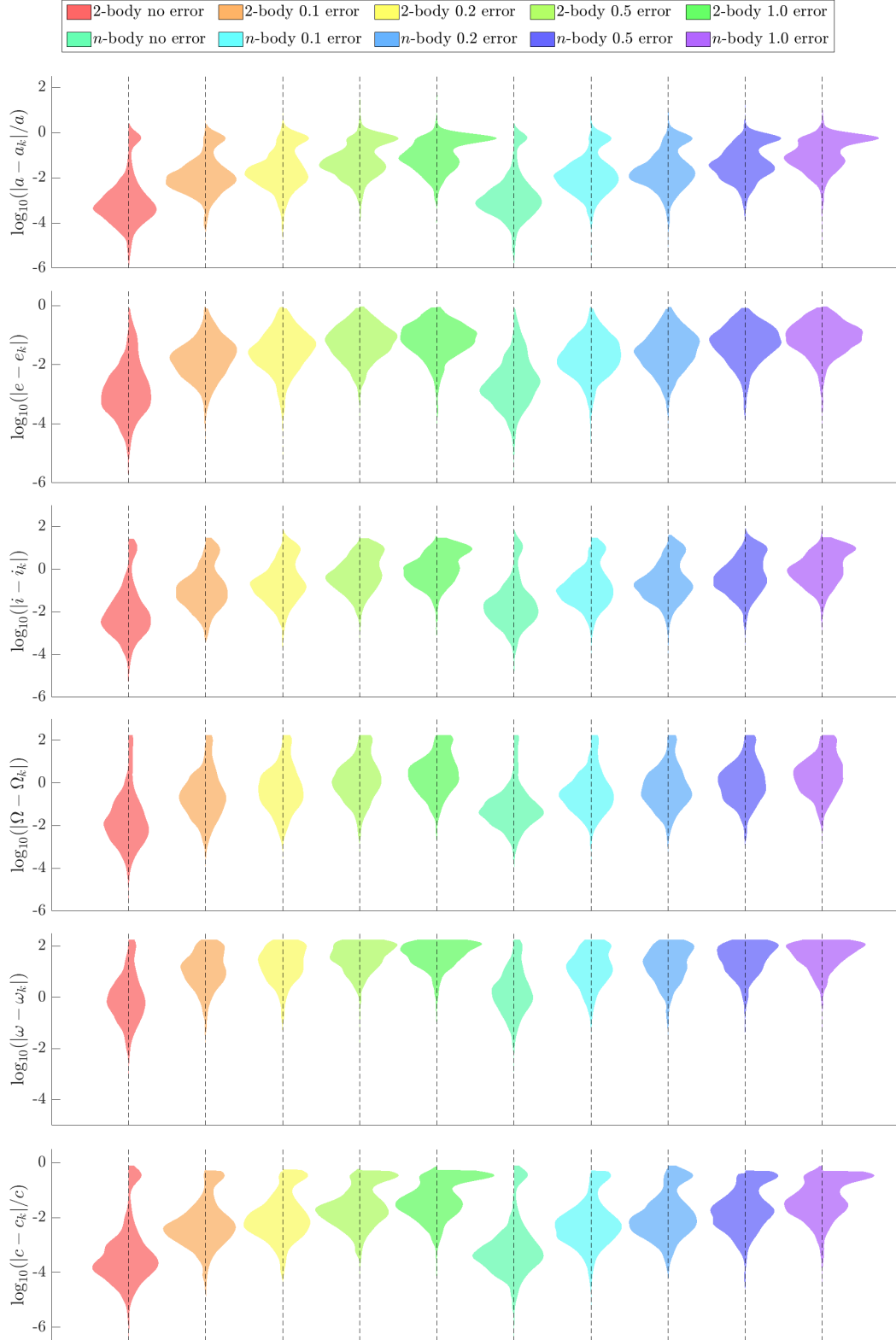


Figure 4: PDF of the logarithm of the error in a , e , i , Ω , ω , and c (top to bottom) for each synthetic data set obtained from the solutions of `link2` (left of the dashed black line) and `link3` (right of the dashed black line).

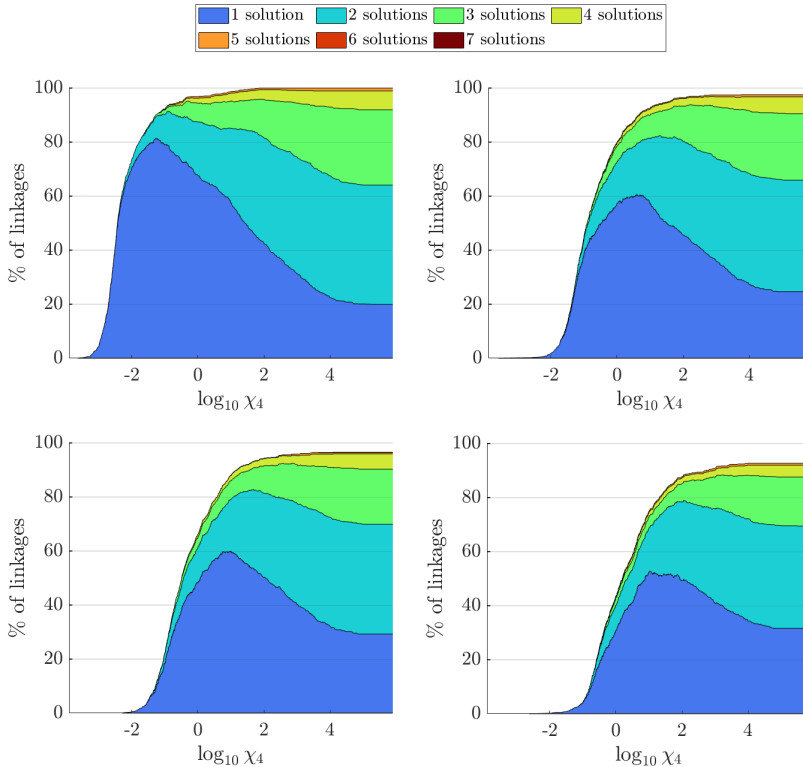


Figure 5: Evolution of the percentage of linkages recovered with a different number of solutions as a function of the χ_4 norm. The synthetic data are generated by a 2-body propagation with no error, and $0.1''$, $0.2''$, $0.5''$ error (from left to right and top to bottom).

one solution. The values of D and χ_4 are correlated which allows us to estimate the quality of a preliminary orbit based only on the value of χ_4 . This is important for processing the ITF where we will not be able to compute D because we will not know the true solution. Similar results are obtained with a 2-body propagation.

With `link3` the correlation between D and Δ_* is even stronger (see Figure 7), thus allowing us to estimate in a better way the quality of preliminary orbits using the value of Δ_* only.

4.1 Time normalisation of the χ_4 norm

From the previous analysis, we found that the Δ_* norm is more correlated with the value of D than the χ_4 norm. Note that the time separation between the tracklets appears in the definition of Δ_* but not in that of χ_4 (see Sections 2.1.1 and 2.2.1 for more details). This is a relevant difference between the two norms since uncertainty accumulates over time. To account for this effect we divide χ_4 by the time separation Δt between the tracklets raised to different powers, i.e. $\chi_4/(\Delta t)^s$ with $s \in \mathbb{R}$. In Figure 8 we plot the correlation of the logarithms of D and $\chi_4/(\Delta t)^s$ as a function of s , for the same data sets used in Figure 6. We see that to maximise the correlation we can take $s \approx 1$. Indeed, the same result still holds for all the synthetic data. We refer to the new norm $\chi_4/\Delta t$ as the normalised χ_4 .

The normalisation of χ_4 by the time separation between the tracklets produces an increase of the linear relation with the logarithm of D (compare Figure 9 with Figure 6).

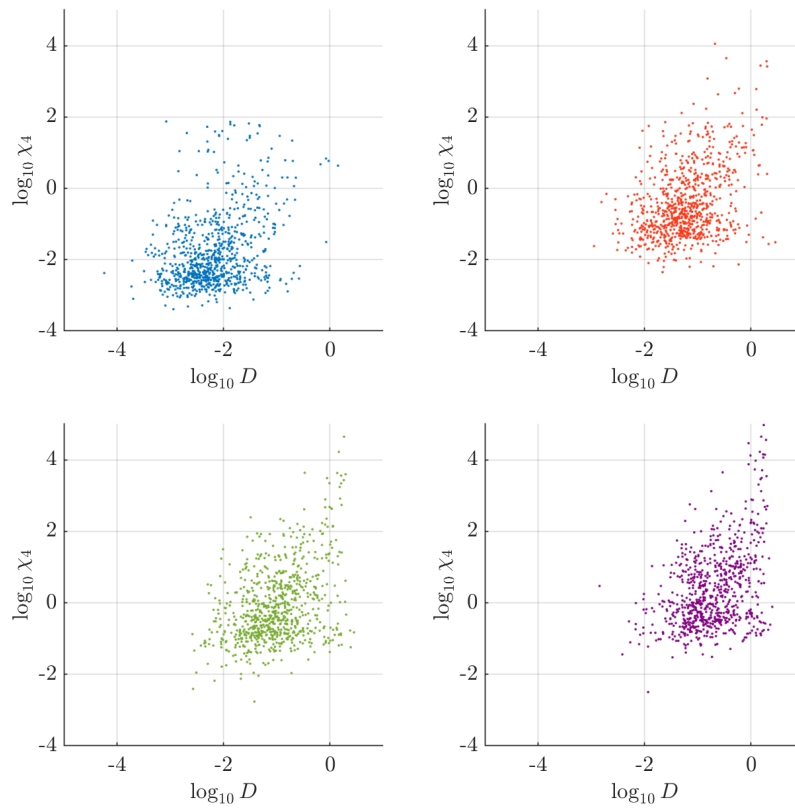


Figure 6: Values of χ_4 vs D in a log-log plot for `link2` using the synthetic data generated by an n -body propagation with no error, and $0.1''$, $0.2''$, $0.5''$ error (from left to right and top to bottom).

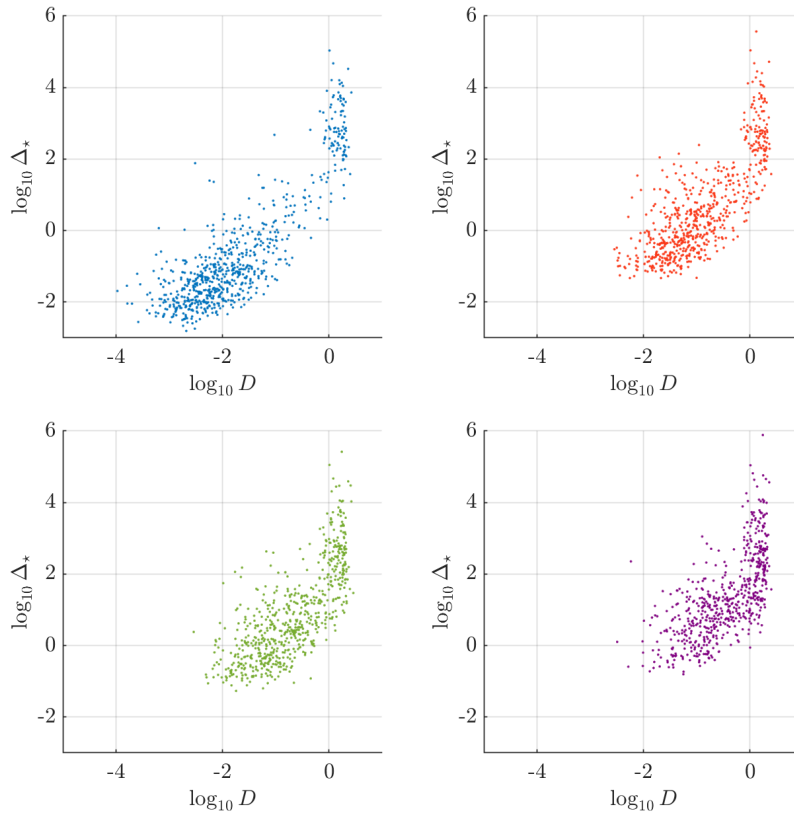


Figure 7: Values of Δ_* vs D in a log-log plot for `link3` using the synthetic data generated by an n -body propagation with no error, and $0.1''$, $0.2''$, $0.5''$ error (from left to right and top to bottom).

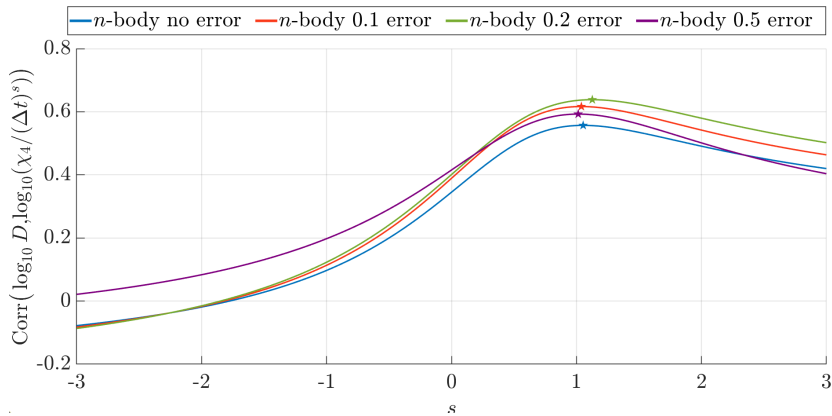


Figure 8: Correlation of the logarithms of D and $\chi_4/(\Delta t)^s$ as a function of s for `link2`. The synthetic data are generated by an n -body propagation with no error, and $0.1''$, $0.2''$, $0.5''$ error.

4.2 The rms of the orbit

Another indicator that can be used to estimate *a priori* the quality of a preliminary orbit is its rms (see Section 2.3) with a 2-body propagation of the orbit.

Figure 10 shows the values of the logarithms of rms and D with `link2` for the same data sets as in Figure 6. If we compare the results of this figure with the similar plots for the normalised χ_4 (see Figure 9) and Δ_* (see Figure 7), we observe that the correlation between the logarithms of rms

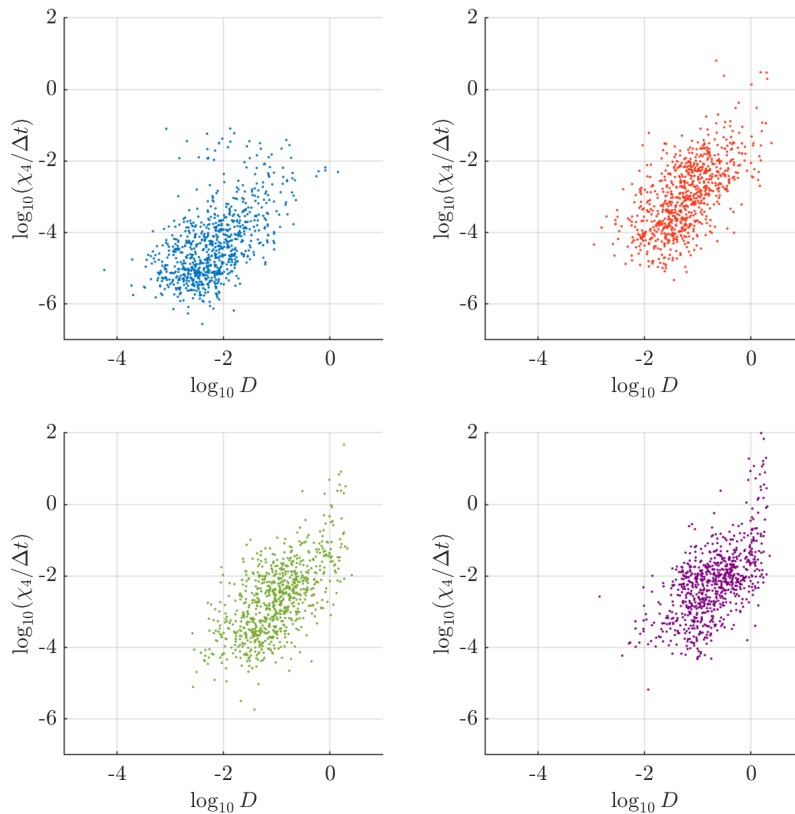


Figure 9: Normalised χ_4 vs D in a log-log plot for `link2`. The synthetic data are generated by an n -body propagation with no error, and $0.1''$, $0.2''$, $0.5''$ error (from left to right and top to bottom).

and D is lower. This is again due to the fact that we do not take into account the time between the tracklets in the computation of the rms . In order to consider this effect, we follow the same strategy used for the normalisation of χ_4 : the rms is divided by the time separation Δt between the tracklets raised to different powers, i.e. $rms/(\Delta t)^s$ with $s \in \mathbb{R}$. From Figure 11 it turns out that the best value of this exponent is $s \approx 3/2$ for all the synthetic data, even if the choice is not so evident as for the χ_4 norm. We will refer to the new norm $rms/(\Delta t)^{3/2}$ as to the normalised rms .

In Figure 12 we present the values of the logarithms of the normalised rms and D with `link2`. Comparison with Figure 10 shows a better correlation when time normalisation is applied.

4.3 Differential corrections of the preliminary orbits

The previous analysis shows that `link2` provides better solutions than `link3`, but an important aspect which has not been explored is whether these preliminary solutions are good enough to obtain least squares orbits, i.e. whether they allow the differential corrections to converge.

We computed a least squares orbit for the best orbit in terms of D obtained with `link2`. More than 97% of the least squares orbits converged when the data had no astrometric error but the percentage decreases as the error increases. The values of the least squares norm R_{LS} (see Section 2.4) are small using synthetic data with no error and increase with the error as expected (see Figure 13).

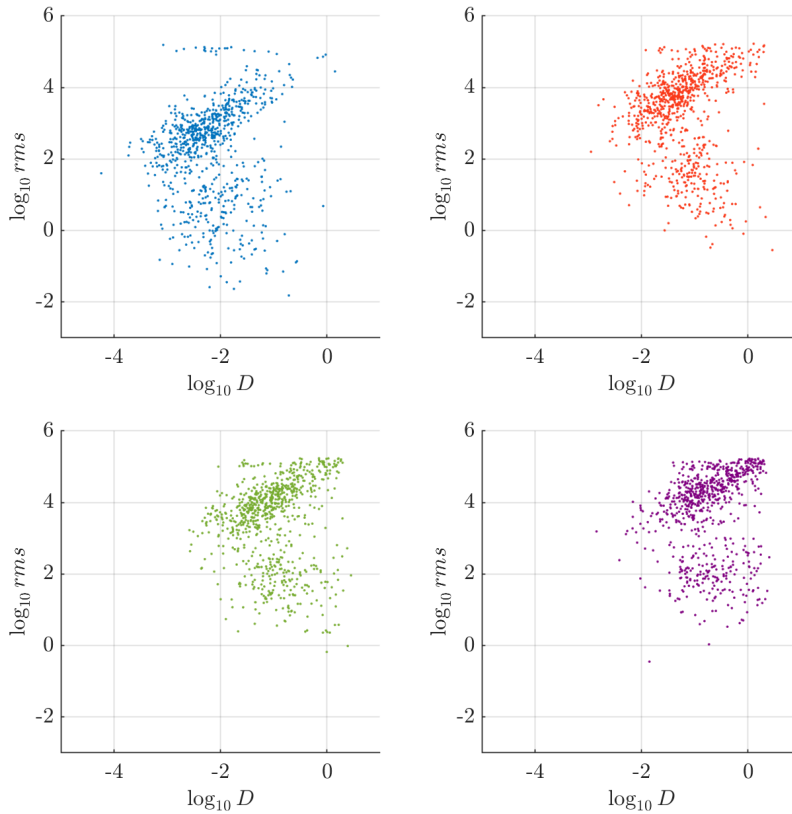


Figure 10: rms vs D in a log-log plot for `link2`. The synthetic data are generated by an n -body propagation with no error, and $0.1''$, $0.2''$, $0.5''$ error (from left to right and top to bottom).

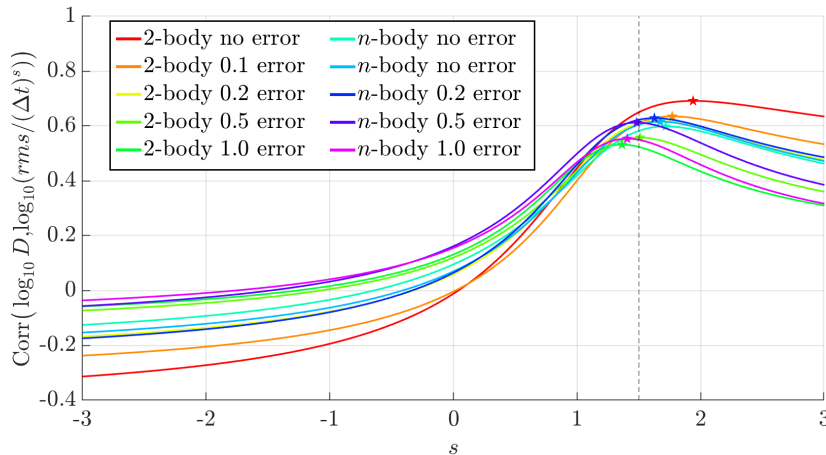


Figure 11: Correlation of the logarithms of D and $rms/(\Delta t)^s$ in terms of s for `link2` applied to all the synthetic data.

4.4 Selection of true linkages

When using the KI methods in practice it can not be known whether tracklets belong to the same object and it is desirable to maximise the number of true linkages while discarding as many of the false ones as possible. For this purpose, we try to link *all* the pairs (for `link2`) and triplets (for `link3`) of tracklets obtainable from those produced for the 822 MBAs.

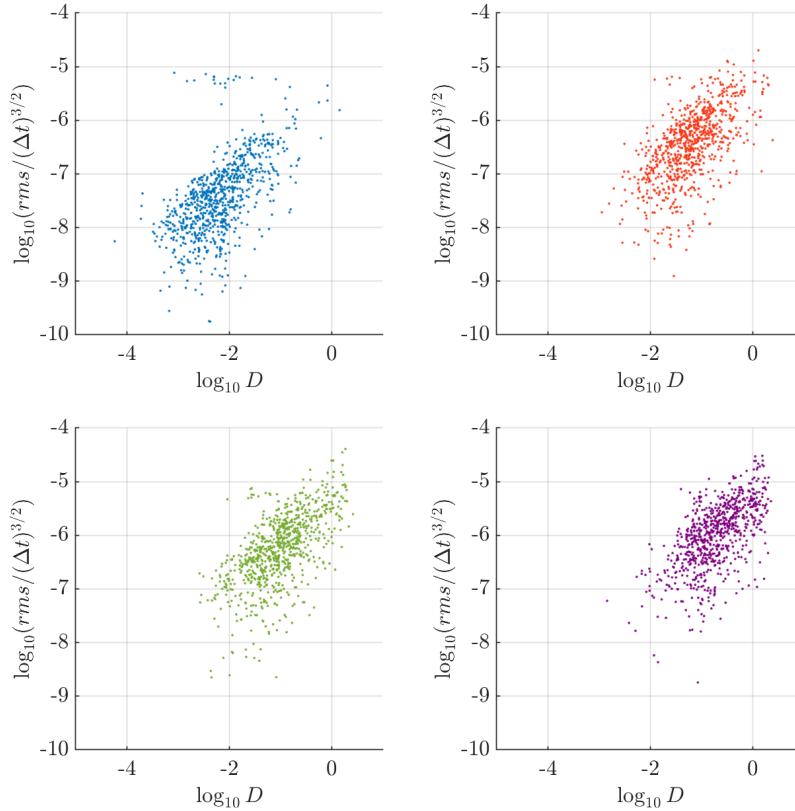


Figure 12: Normalized rms vs D in a log-log plot for `link2`. The synthetic data are generated by an n -body propagation with no error, and $0.1''$, $0.2''$, $0.5''$ error (from left to right and top to bottom).

Figure 14 shows a clear separation in terms of χ_4 between true and false linkages for observations with no error, but the separation decreases as the error increases both with the 2-body and the n -body dynamics.

The selection of a threshold for the χ_4 norm requires care. For example, in the case with no error (Figure 14) it appears that a suitable value for $\log_{10} \chi_4$ is 0, however this choice would provide an overwhelming number of false linkages. It is evident in the PDF of $\log_{10} \chi_4$ for the false linkages using a logarithmic scale on the vertical axis (see Figure 15). On the other hand, a smaller threshold, around -1.4 , yields only a few outliers, but we expect that even this threshold will generate many false linkages in large datasets, such as the ITF. In addition, since the PDF of $\log_{10} \chi_4$ for false linkages remains almost unchanged as the astrometric error increases, this threshold excludes more true solutions as the error increases, see Figures 14 and 6. Of course, increasing the threshold will generate more false linkages. Similar conclusions can be drawn for the normalised χ_4 , but for the same number of false linkages we recover less true ones.

The results obtained with `link3` are similar to `link2`. In Figure 16 we observe a clear separation in terms of the value of Δ_* between the solutions of the true (green) and false (yellow and red) linkages considering synthetic data with no astrometric error. The separation decreases as we increase the error.

The PDFs of the false solutions are a bit different if the tracklets belong to two or three different objects (see Figure 16), as expected, because the latter case is “more wrong” than the former. In

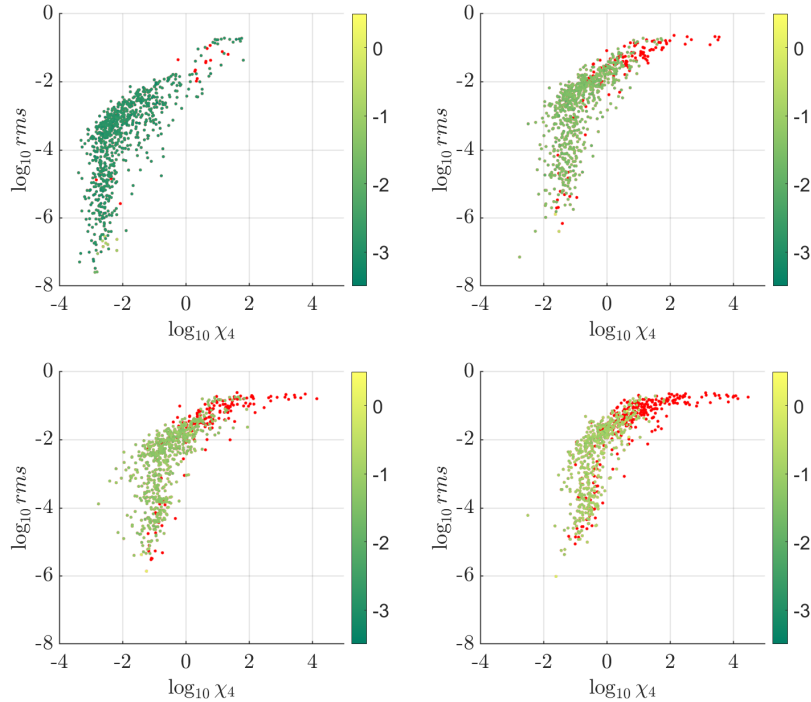


Figure 13: rms vs χ_4 in a log-log plot for the solutions of `link2` and logarithmic values of R_{LS} (green scale) of the least squares orbits obtained from these solutions. The synthetic data are generated by an n -body propagation with no error, and $0.1''$, $0.2''$, $0.5''$ error (from left to right and top to bottom). The red dots correspond to preliminary orbits that do not converge in the differential corrections scheme.

particular, in Figure 17 we show in a log-log plot the PDFs of Δ_* for the false linkages corresponding to the yellow (left) and red (right) distributions of Figure 16.

Selecting a threshold around -0.5 we have only a few outliers. However, like for `link2`, with such a small threshold we lose a high percentage of true solutions when we include the astrometric error.

Regarding the distribution of the rms of the solutions we have a similar situation: the separation between the true and false linkages is clear when we consider data sets with no error and it decreases with increasing astrometric error (see Figure 18 for the results obtained with `link2`). Moreover, similar to the case with the normalised χ_4 , the normalised rms shows a worse separation between true and false solutions.

A combination of all the metrics introduced so far can be used to discard *a priori* (that is, before applying the differential corrections scheme) as many false solutions as possible. For example, in Figure 19 the non-normalised (left plot) and normalised (right plot) metrics could be used to discard some false linkages. In fact, in the left plot there is a more clear separation between true and false solutions, while in the right one the true solutions are gathered in a smaller region of the plane.

Before concluding this section, it is important to note that discarding false linkages *a priori* is necessary, because the combinatorics in large data sets (e.g. the ITF) would require enormous computing power if all the possible solutions are to be considered (see section 6). Nevertheless, when differential corrections are applied to false linkages starting with `link2`'s preliminary solutions more than 98% do not converge. We also note that all the preliminary solutions with $\log_{10} \chi_4$ greater

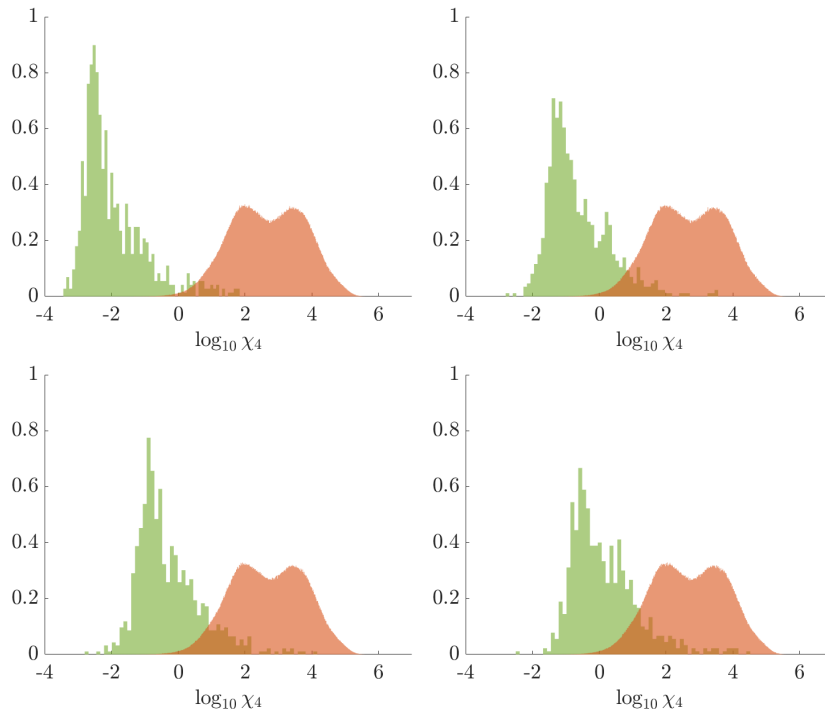


Figure 14: PDF of the logarithm of χ_4 for the true (green) and false (red) linkages of `link2`. The synthetic data are generated by an n -body propagation with no error, and $0.1''$, $0.2''$, $0.5''$ error (from left to right and top to bottom).

than 4.3 do not converge. Finally, the separation in the value of R_{LS} for the solutions obtained from the true and false linkages is quite clear when there is no error, and it decreases as the astrometric error increases (see Figure 20).

5 Testing the KI methods with real data

In this section we study the behaviour of `link2` and `link3` using real observations from the Pan-STARRS1 telescope.

5.1 The error distribution for real observations

Working with real observations we can not assume that the astrometric errors are independently distributed following a 2d Gaussian distribution as in the case of the synthetic observations [see for example 1, 2].

The astrometric error was introduced in the synthetic observations by applying the following procedure. First, we simulate perfect observations (α_i^*, δ_i^*) using 2-body or n -body propagation. Then, we select a random angle, $\theta \in [0, 2\pi)$, representing a direction on the tangent plane to the celestial sphere, and change the observations following a Gaussian distribution in that direction. In this way, the astrometric error in the observation (α_i, δ_i) , that we define as

$$e_i = \text{sign}(\Delta_{\alpha_i}) \sqrt{\Delta_{\alpha_i}^2 \cos^2 \delta_i + \Delta_{\delta_i}^2}, \quad (8)$$

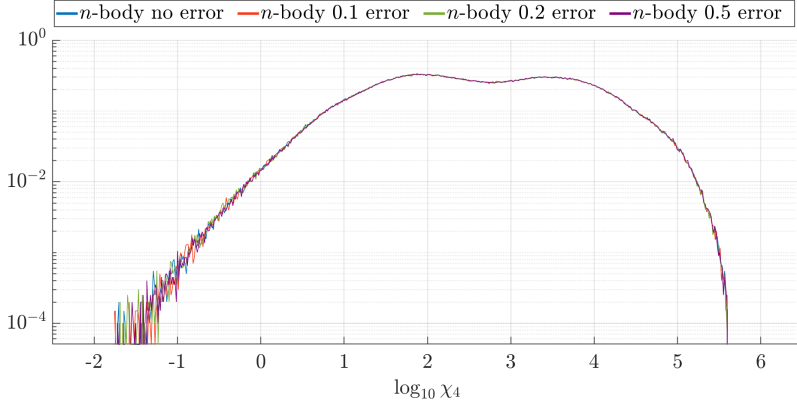


Figure 15: PDF of the logarithm of χ_4 for false linkages using `link2`. The synthetic data are generated by an n -body propagation with no error and $0.1''$, $0.2''$, $0.5''$ error.

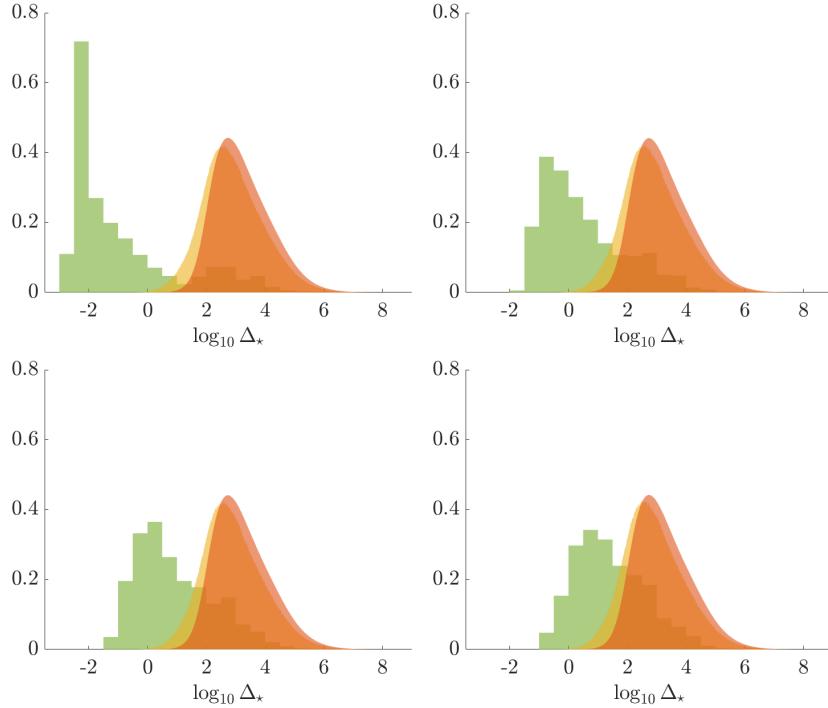


Figure 16: PDF of the logarithm of Δ_* for the true (green) linkages of `link3` and the false ones with two tracklets belonging to the same object (yellow) and each tracklet belonging to different objects (red). The synthetic data are generated by a 2-body propagation with no error, and $0.1''$, $0.2''$, $0.5''$ error (from left to right and top to bottom).

where $\Delta_{\alpha_i} = \alpha_i^* - \alpha_i$ and $\Delta_{\delta_i} = \delta_i^* - \delta_i$, follows a normal distribution with zero mean and standard deviation σ in the synthetic data (see for example the left and middle plots in Figure 21).

The error in the real observations is estimated from equation (8), where the perfect observations (α_i^*, δ_i^*) are calculated by a full n -body propagation [8] which also includes the effect of the largest asteroids. The resulting distribution of the errors looks like a Gaussian (see the right plot of Figure 21), and its mean and standard deviation are given in Table 1. However, the important difference with respect to the synthetic data is the correlation of the errors in observations within the same tracklet which is no longer negligible. Indeed, in the case of real data there is a significant correlation (> 0.5) between the errors of two observations randomly selected from the same tracklet (see Table

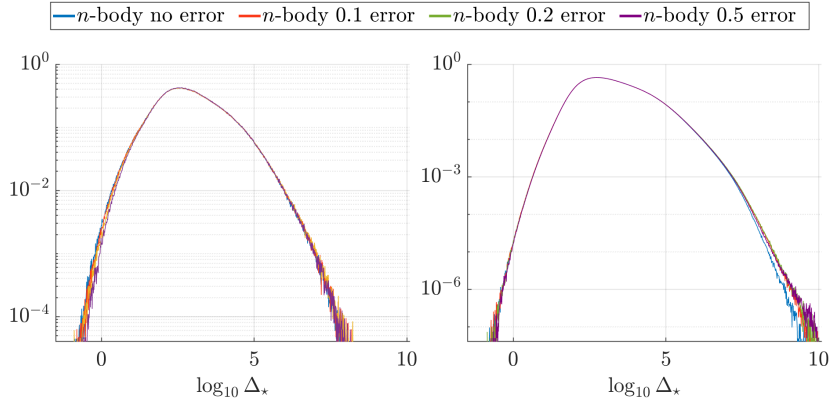


Figure 17: PDF of the logarithm of Δ_\star for the false linkages of `link3` with two tracklets belonging to the same object (left) and each tracklet belonging to different objects (right). The synthetic data are generated by a 2-body propagation with no error, and $0.1''$, $0.2''$, $0.5''$ error.

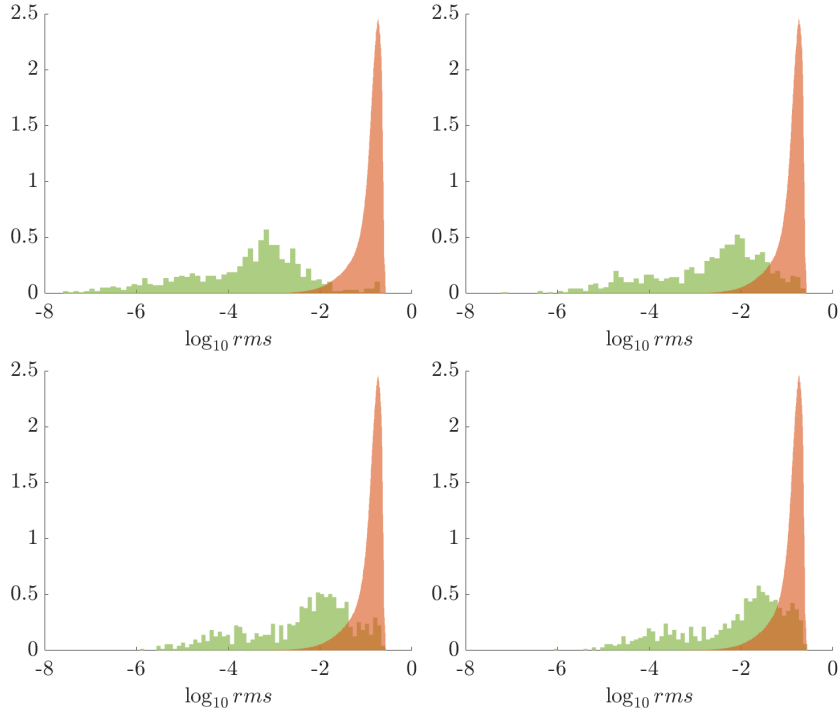


Figure 18: PDF of the logarithm of the rms for the true (green) and false (red) linkages of `link2`. The synthetic data are generated by an n -body propagation with no error, and $0.1''$, $0.2''$, $0.5''$ error (from left to right and top to bottom).

Dataset	Expec. μ	Compu. μ	Expec. σ	Compu. σ
n -body 0.1	0	0.0073	0.1	0.1088
n -body 0.2	0	0.0037	0.2	0.2099
real	-	0.0593	-	0.2227

Table 1: Statistics of the distribution of the astrometric error (values are in arcsec).

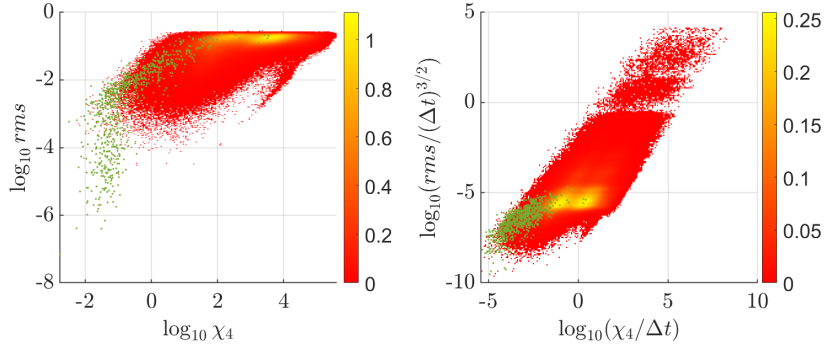


Figure 19: Left: rms vs χ_4 in a log-log plot for the true (green) and false (hot colours) linkages of `link2`. The colour scale refers to the values of the PDF of the number of false linkages. The synthetic data are generated by an n -body propagation with $0.1''$ error. Right: the same as in the left plot but for the normalised rms and normalised χ_4 .

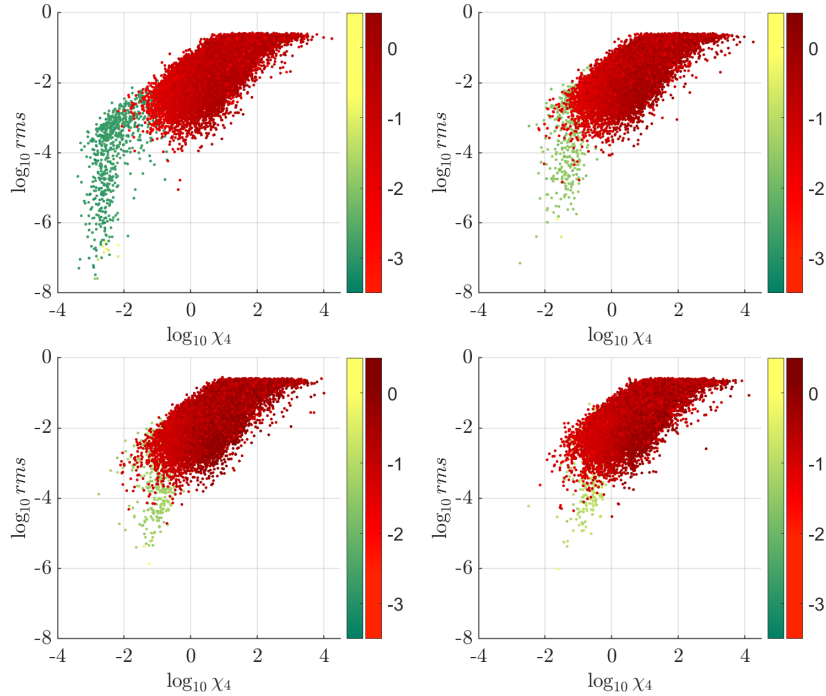


Figure 20: rms vs χ_4 in a log-log plot for the solutions of `link2` and logarithmic values of R_{LS} of the least squares orbits obtained from the true (green scale) and false (red scale) solutions. The synthetic data are generated by an n -body propagation with no error, and $0.1''$, $0.2''$, $0.5''$ error (from left to right and top to bottom).

2). This means that the values of the indicators (χ_4 , Δ_* , rms) will be distributed differently for real observations compared to synthetic ones, since we also assume that the astrometric error is uncorrelated in the construction of the attributables.

	n -body $0.1''$	n -body $0.2''$	real
Correlation	0.0365	0.0458	0.5206

Table 2: Correlation of the errors in the observations that belong to the same tracklet.

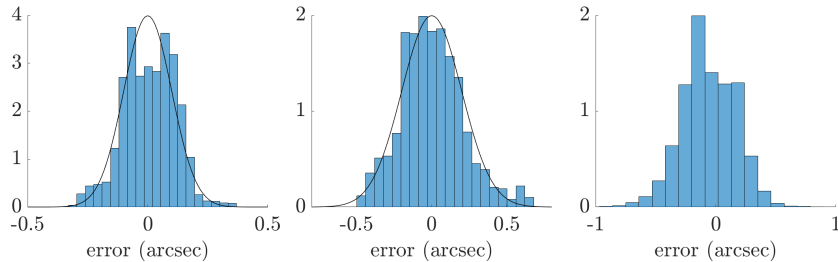


Figure 21: Normalised histograms of the astrometric error for the synthetic data generated by an n -body propagation with $0.1''$ and $0.2''$ error, and for the real data (from left to right). The black curve in the left and middle plots represents the normal distribution with zero mean and standard deviation of $0.1''$ and $0.2''$, respectively.

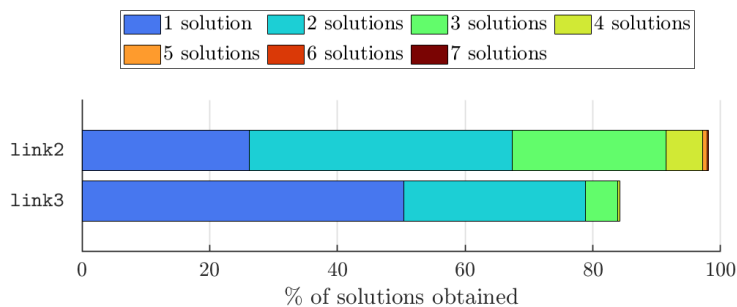


Figure 22: Percentage of linkages and multiplicity of the solutions obtained by `link2` and `link3` with the real data set.

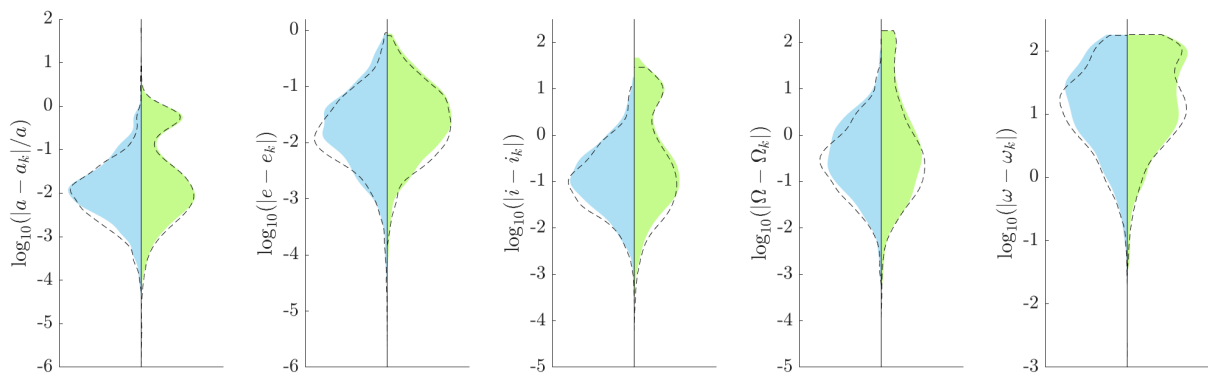


Figure 23: PDF of the logarithm of the error in a , e , i , Ω , and ω (from left to right) for the solutions obtained by `link2` (blue) and `link3` (green) on the real data set. The dashed lines correspond to the PDFs for the synthetic data set generated by an n -body propagation with $0.2''$ error.

5.2 Numerical results

We now examine the performance of our `link2` and `link3` algorithms on real data.

The percentage of true linkages recovered by each method (Figure 22) is similar to the results obtained with synthetic data with an astrometric error of $0.2''$ (see Figure 3). In addition, the quality of the solutions (i.e. the error in the orbital elements a, e, i, Ω, ω) is similar (see Figure 23) and reassures us that it is suitable to employ synthetic data to study the behaviour of both

methods. On the other hand, the χ_4 and Δ_\star norms for the real data are larger than those in the synthetic data case with $0.2''$ error (compare Figure 24 with Figures 6 and 7) because the errors in the real observations within a tracklet are not independent.

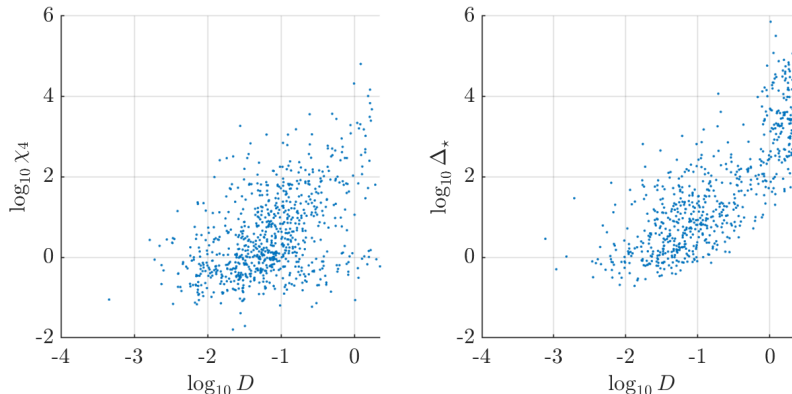


Figure 24: Left: χ_4 vs D in a log-log plot for `link2` with real data. Right: Δ_\star vs D in a log-log plot for `link3` with real data.

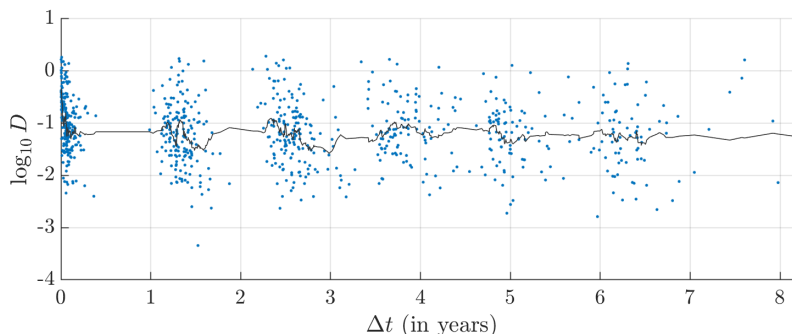


Figure 25: Value of the D -criterion of the preliminary orbits obtained by `link2` with the real data as a function of the time separation between the tracklets.

Note that both methods are able to link tracklets with a large time separation and produce preliminary solutions quite close to the real orbits even when the tracklets are separated by a few years. In Figure 25 we plot the value of the D -criterion of the preliminary orbits obtained with `link2` in terms of the time separation between the tracklets. Moreover, we draw a black curve corresponding to the *simple moving average* $\text{SMA}_{25,12}$, made with 25 data points, 12 on the left and 12 on the right of the central value, when they are available. When the central value is close to the boundary we use all the available data points within these limits. Note that the values of $\text{SMA}_{25,12}$ keep below the -0.7 threshold of the similarity criterion.

Differential corrections were then applied to the best solutions (in terms of D) of the two KI methods obtained with true linkages in the real data. The values of the *rms* of the least squares orbits (R_{LS}) are shown in Figure 26. More than 80% of the `link2` preliminary solutions converge to a least squares orbit but, due to the correlations in the observational errors, the values of R_{LS} are larger using real data than the synthetic data set with $0.2''$ error.

As expected, the least squares orbits are better than the preliminary ones, not only in terms of D but also in the error of each orbital element, see Figure 27. In this figure we also observe that the orbits that do not converge are affected by larger errors in the orbital elements.

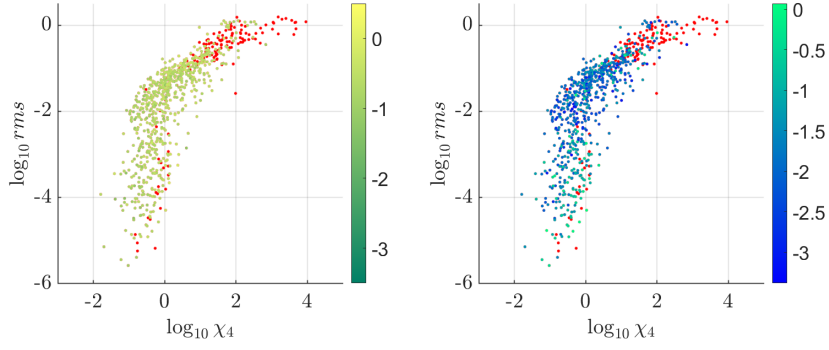


Figure 26: rms vs χ_4 in a log-log plot for the solutions of `link2` using real data and logarithmic values of R_{LS} (green scale, left plot) and D (blue scale, right plot) of the least squares orbits obtained from these solutions. The red dots correspond to preliminary orbits that do not converge in the differential corrections scheme.

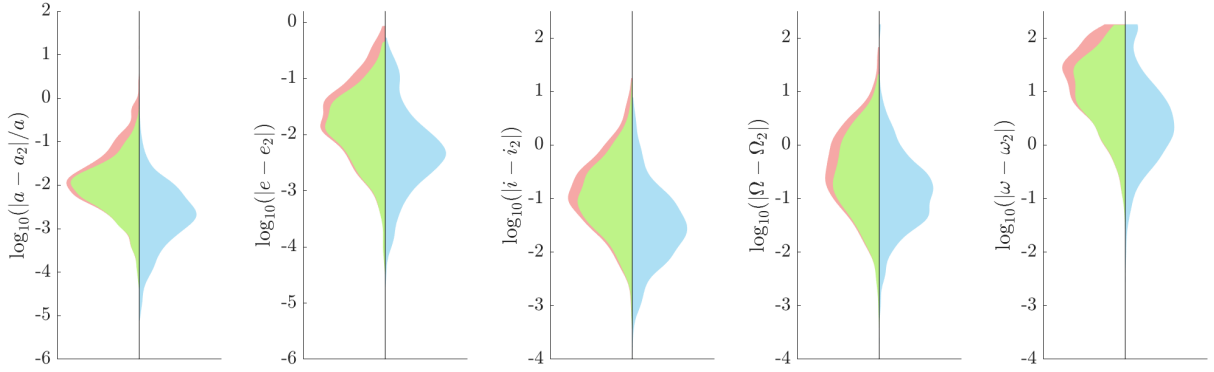


Figure 27: PDF of the logarithm of the error in a , e , i , Ω , and ω (from left to right) for the solutions of `link2` that converge (green) and do not converge (red) to a least squares orbit using real data. In blue the same PDFs are shown for the least squares orbits.

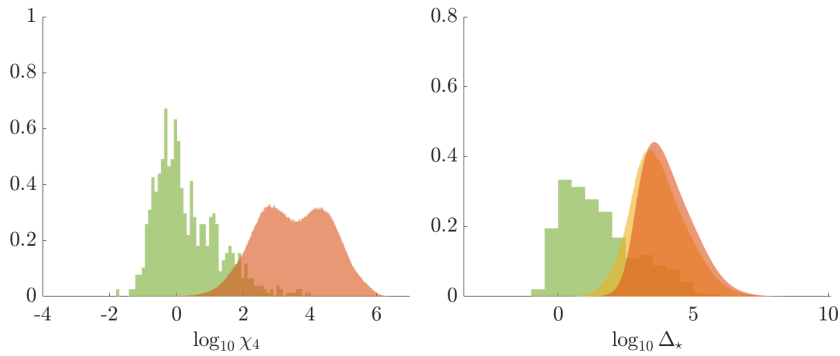


Figure 28: Left: PDF of the logarithm of χ_4 for the true (green) and false (red) linkages of `link2` using real data. Right: PDF of the logarithm of Δ_* for the true (green) linkages of `link3` and the false ones with two tracklets belonging to the same object (yellow) and each tracklet belonging to different objects (red) using real data.

Next, we investigate the ability of the KI methods to recover true linkages when applied to real observations. For this purpose, we apply the same test that we performed with the synthetic data

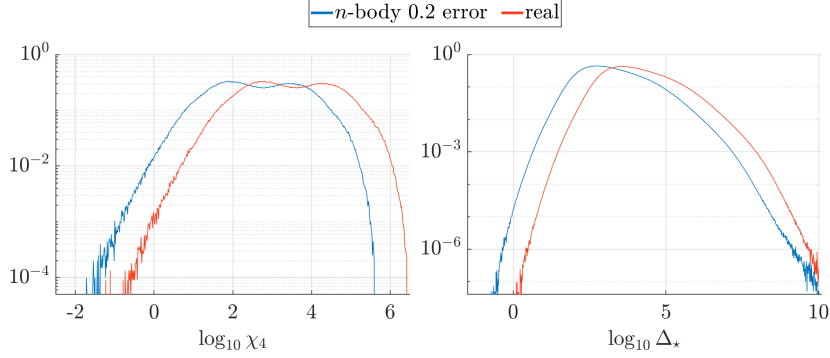


Figure 29: Left: PDF of the logarithm of χ_4 for the false linkages of `link2` using the synthetic data set generated by an n -body propagation with $0.2''$ error (blue) and the real data (red). Right: the same for the PDF of the logarithm of Δ_* with `link3`.

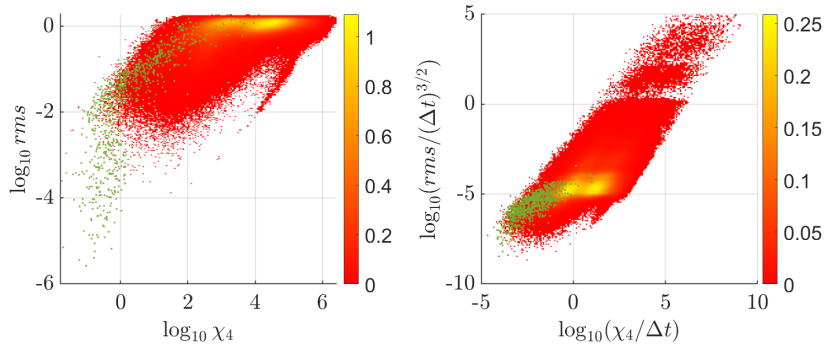


Figure 30: Same as in Figure 19 but for real observations.

sets (see Section 4.4). In Figure 28 we show the PDF of the χ_4 and Δ_* norms for true and false linkages. These distributions are almost identical to those obtained for synthetic observations with $0.2''$ error (see for comparison the corresponding plots in Figures 14 and 16), but they all have a small positive displacement in the horizontal axis.

This phenomenon can also be observed from the comparison of Figures 30 and 19 and from Figure 31.

We emphasise that in this case near the 99% of false linkages do not converge to a LS orbit when we apply the differential corrections. We also note that all the preliminary solutions with $\log_{10} \chi_4$ greater than 5 do not converge.

In conclusion, when dealing with real observations we can set the thresholds of χ_4 and Δ_* by properly increasing the values of these two norms previously found with the synthetic populations (see Figure 29).

6 Application to the ITF

One of our future goals is to apply the KI methods to the MPC's ITF to identify tracklets that can be associated with known objects and to discover unknown objects with tracklets that have not been linked together. In this section we estimate bounds on the technique's efficiency with some assumptions on the data's characteristics and the method's application.

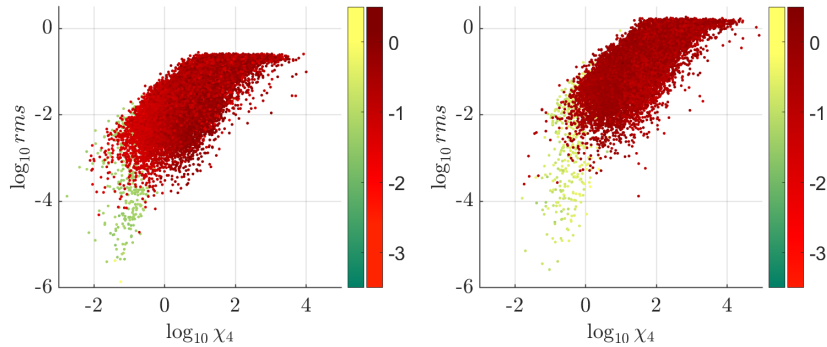


Figure 31: rms vs χ_4 in a log-log plot for the solutions of `link2` and logarithmic values of R_{LS} of the least squares orbits obtained from the true (green scale) and false (red scale) solutions using synthetic observations generated by an n -body propagation with $0.2''$ error (left) and real observations (right).

First, we assume that the application to the ITF will use `link2` since it has a higher efficiency at recovering true linkages than `link3` (98% vs. 84% for real observations) and the quality of its solutions is good.

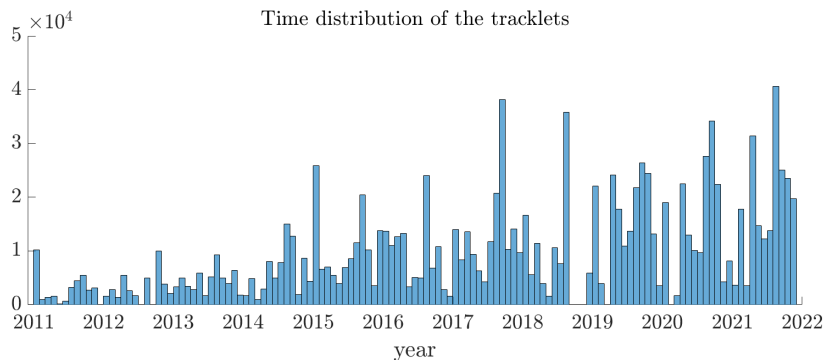


Figure 32: Distribution of the average time of observation of Pan-STARRS1 tracklets containing ≥ 3 detections in the ITF.

Second, for the purpose of this calculation, and to ensure that the data has consistent properties, e.g. astrometric and photometric accuracy, we only consider ITF tracklets containing ≥ 3 detections contributed by Pan-STARRS1 which dominates the ITF at almost 50% of the total number of tracklets. This data set contains $N = 1,252,187$ tracklets so it is about 760 times larger than the synthetic and real data sets used with `link2` in the previous sections and its time distribution can be observed in Figure 32. The increasing number of unlinked tracklets as a function of time is likely due to Pan-STARRS1 modifying its survey strategy and incremental improvements in system operations [3].

Since the computational cost of a full numerical exploration is $\mathcal{O}(N^2)$, where N is the number of tracklets in the data set, the time of computation and the number of (true and false) solutions of `link2` will increase by a factor $\approx 580,000$ relative to the cost of exploring our small subset of real Pan-STARRS1 ITF data (see Table 3).

The identification of a new object in the ITF will require linking ≥ 4 tracklets. The combinatorics of linking tracklets within the ITF can be expressed as a graph $G = G(V, E)$ where V , the set of vertices, corresponds to the set of tracklets (i.e. $V = \{1, 2, \dots, N\}$) and E , the set of edges, corresponds to the linkages, i.e. we will consider $e_{ij} \in E$ with $i, j \in V$ if and only if we obtain

	real data	ITF F51 data
Number of solutions	1,861,785	$\approx 1.08 \cdot 10^{12}$

Table 3: Total number of solutions (true and false, including multiple solutions, without setting a threshold for χ_4) generated by `link2` with the real data set of 822 objects used in this work (Section 5) and the expected total number of solutions with Pan-STARRS1 (F51) tracklets extracted from the ITF.

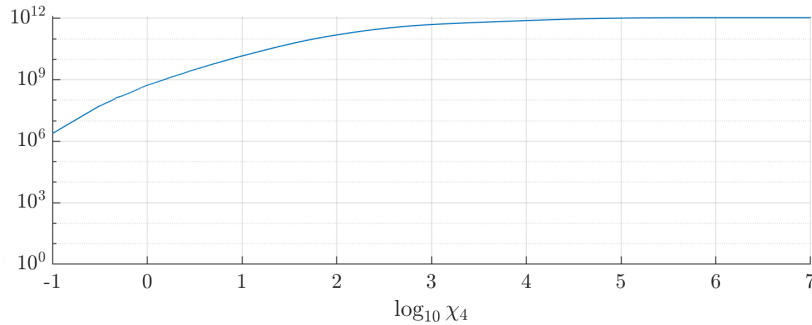


Figure 33: Expected number of solutions as a function of the threshold of the logarithm of χ_4 for the set of Pan-STARRS1 (F51) tracklets contained in the ITF.

a linkage between the tracklets i and j using `link2`. Thus, we need to estimate the number of 4-connected sub-graphs of G .

To that end we define the random variable X_{ij} as a function of the threshold value χ_4^* of χ_4 :

$$X_{ij}(\chi_4^*) = \begin{cases} 1 & \text{if we obtain at least one solution for the tracklets} \\ & i \text{ and } j \text{ with } \chi_4 \leq \chi_4^*, \\ 0 & \text{otherwise,} \end{cases}$$

so $X_{ij} = 1$ if $e_{ij} \in E$, and $X_{ij} = 0$ otherwise.

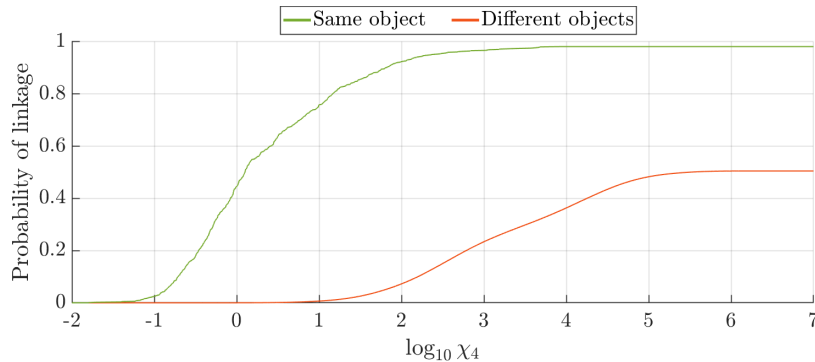


Figure 34: Probability of obtaining a preliminary orbit with `link2` if two tracklets belong to the same object (green) or not (red), as a function of the threshold value of χ_4 .

From the previous analysis, we can estimate the probability $P(X_{ij} = 1)$ as a function of χ_4^* , taking also into account whether the tracklets i and j belong or not to the same object. These results can be observed in Figure 34. We note that the probability to obtain a linkage with 2 tracklets belonging to different objects gets very close to 0.5 as χ_4 increases.

It is important to note that we do not know the distribution of the number of tracklets per object

in the ITF and therefore we cannot determine the number of 4-connected sub-graphs that will be found. To set a lower bound on the problem we assume that there is a single object with 4 tracklets in the ITF and the rest of the $N - 4$ tracklets belong to $N - 4$ different objects. Furthermore, we assume that the linkages are independent i.e. there is no correlation between the `link2` solutions of pairs or tracklets belonging to the same object.

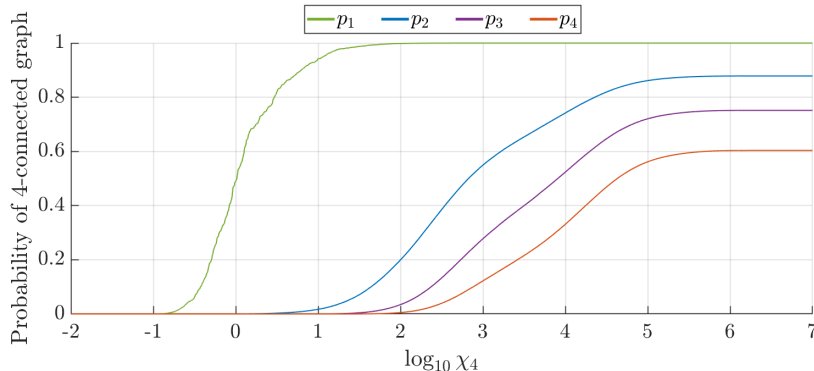


Figure 35: Probability p_k of identifying a 4-connected sub-graph given 4 tracklets that belong to $k = 1, \dots, 4$ different objects as a function of the χ_4 threshold.

To calculate the number of 4-connected sub-graphs that must be tested, let us define p_k as the probability that 4 tracklets belonging to $k = 1, \dots, 4$ different objects form a 4-connected subgraph. The values of p_k as a function of χ_4 are shown in Figure 35 (see more details in Appendix A). As the χ_4 threshold is loosened the probability of identifying the correctly linked 4-connected sub-graph increases quickly around $\log_{10} \chi_4 = 0$ and by $\log_{10} \chi_4 = 1$ there is nearly 100% probability that the set of 4 tracklets will be identified. On the other hand, the probability that 1 of the 4 tracklets will be an unrelated interloper begins to increase around $\log_{10} \chi_4 = 1$ and by $\log_{10} \chi_4 \approx 3$ the probability that all 4 tracklets are unrelated is $> 10\%$.

In this way, the expected number (N_4) of 4-connected sub-graphs in the data set as a function of χ_4 is given by (see Appendix A)

$$N_4(\chi_4) = p_1 + 4(N - 4)p_2 + 6\binom{N - 4}{2}p_3 + \left[4\binom{N - 4}{3} + \binom{N - 4}{4}\right]p_4. \quad (9)$$

Since each p_k is an increasing function of χ_4 we can calculate the probability of detecting the single set of 4 tracklets corresponding to the same object as a function of the number of sets of 4 tracklets that must be tested (i.e. the number of 4-connected sub-graphs N_4), see Figure 36.

Since we expect that the ITF contains more than one object that has at least 4 tracklets, Figure 36 provides a lower bound on the number of 4-tracklets sets that must be tested to recover the desired fraction of unidentified objects (i.e. the value of p_1 , in our simple case).

These results may seem discouraging because they suggest that we will need to test more than 10^{15} sets of 4-tracklets to recover at least 80% of the objects and that number of differentially corrected orbit computations would be challenging. Thus, we will need to invoke extra conditions on the 4-tracklets before attempting a least squares orbit to drastically reduce the computational problem. We expect that the `link2` preliminary orbit solutions will provide the necessary reduction by requiring that pairs of tracklets in the set of connected tracklets have similar Keplerian integrals.

We will further develop this technique in its application to the ITF in our next paper, but it is

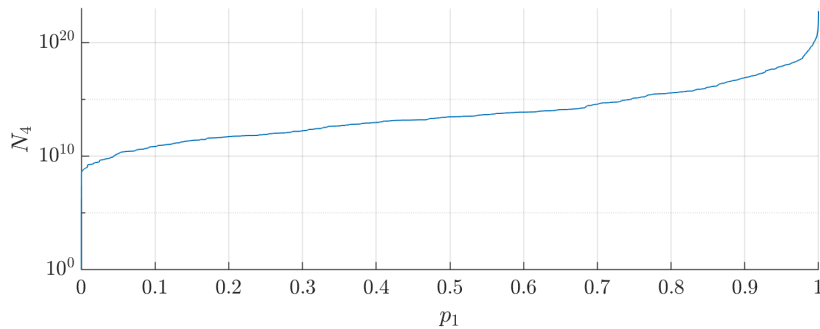


Figure 36: Expected number of 4-connected sub-graphs that must be tested as a function of the probability, p_1 , of identifying the correctly linked set of 4 tracklets.

clear that achieving detection efficiencies of $> 90\%$ for objects with just 4-tracklets in the ITF is a challenging task.

7 Conclusions

Two linkage methods for initial orbit determination, named `link2` and `link3`, have been analysed using synthetic and real data, with the goal of understanding whether they can be efficiently applied to large repositories of unlinked detections, such as the MPC’s ITF. The low computational cost of these algorithms make them promising for this purpose.

The results obtained with synthetic data generated with astrometric errors typical of modern wide-field asteroids surveys are good: the percentage of recovered true linkages is high, and the preliminary orbits are close to the real ones. In these two aspects `link2` is better than `link3`. Furthermore, the orbital plane is quite well determined by both methods. On the other hand, the percentage and the quality of the solutions decrease for larger astrometric error.

Some indicators to estimate the quality of the preliminary solutions have been studied. These indicators, χ_4 for `link2`, Δ_* for `link3` and the *rms* of the orbit for both methods, show a significant correlation with the quality of the preliminary orbits, which was quantified with the *D*-criterion. By setting suitable thresholds for these indicators a large fraction of the false linkages, which are unavoidably produced with both methods, can be discarded, without losing too many true ones. This operation is less effective as the error increases.

Using some simple assumptions we have seen that a preliminary exploration of the ITF is computationally feasible with a procedure relying on `link2`. For this reason, we believe that `link2` is a good method to carry out a complete exploration of the ITF observations made by Pan-STARRS1.

Acknowledgments

This work was partially supported through the H2020 MSCA ETN Stardust-Reloaded, Grant Agreement Number 813644. OR acknowledges the Spanish MINECO/FEDER grant PGC2018-100928-B-I00. GFG and GB also acknowledge the project MIUR-PRIN 20178CJA2B “New frontiers of

Celestial Mechanics: theory and applications" and the GNFM-INdAM (Gruppo Nazionale per la Fisica Matematica). Part of this work was performed during RJ's visits in Pisa.

Data Availability

The data underlying this article will be shared on reasonable request to the corresponding author.

References

- [1] J. Baer, S. R. Chesley, and A. Milani. "Development of an observational error model". In: *Icarus* 212.1 (Mar. 2011), pp. 438–447. DOI: 10.1016/j.icarus.2010.11.031.
- [2] M. Carpino, A. Milani, and S. R. Chesley. "Error statistics of asteroid optical astrometric observations". In: *Icarus* 166.2 (Dec. 2003), pp. 248–270. DOI: 10.1016/S0019-1035(03)00051-4.
- [3] K. C. Chambers, E. A. Magnier, N. Metcalfe, H. A. Flewelling, et al. *The Pan-STARRS1 Surveys*. 2019. arXiv: 1612.05560 [astro-ph.IM].
- [4] E. J. Christensen, D. Carson Fuls, A. Gibbs, A. Grauer, et al. "The Catalina Sky Survey for Near-Earth Objects". In: *AAS/Division for Planetary Sciences Meeting Abstracts #48*. Vol. 48. AAS/Division for Planetary Sciences Meeting Abstracts. Oct. 2016, 405.01, p. 405.01.
- [5] L. Denneau, R. Jedicke, T. Grav, M. Granvik, et al. "The Pan-STARRS Moving Object Processing System". In: *PASP* 125 (Apr. 2013), pp. 357–395. DOI: 10.1086/670337. arXiv: 1302.7281 [astro-ph.IM].
- [6] J. D. Drummond. "The D Discriminant and Near-Earth Asteroid Streams". In: *Icarus* 146 (2 Aug. 2000). DOI: 10.1006/icar.2000.6401.
- [7] C. F. Gauss. *Theoria motus corporum in sectionibus conicis solem ambientium*. Reprinted by Dover publications in 1963, 1809.
- [8] M. Granvik, J. Virtanen, D. Oszkiewicz, and K. Muinonen. "OpenOrb: Open-source asteroid orbit computation software including statistical ranging". In: *Meteoritics and Planetary Science* 44 (Jan. 2009), pp. 1853–1861. DOI: 10.1111/j.1945-5100.2009.tb01994.x.
- [9] G. F. Gronchi, G. Baù, and S. Marò. "Orbit determination with the two-body integrals. III". In: *Cel. Mech. Dyn. Ast.* 123/2 (2015), pp. 105–122.
- [10] G. F. Gronchi, G. Baù, and A. Milani. "Keplerian integrals, elimination theory and identification of very short arcs in a large database of optical observations". In: *Cel. Mech. Dyn. Ast.* 127/2 (2017), pp. 211–232.
- [11] G. F. Gronchi, L. Dimare, and A. Milani. "Orbit determination with the two-body integrals". In: *Cel. Mech. Dyn. Ast.* 107/3 (2010), pp. 299–318.
- [12] G. F. Gronchi, D. Farnocchia, and L. Dimare. "Orbit determination with the two-body integrals. II". In: *Cel. Mech. Dyn. Ast.* 110/3 (2011), pp. 257–270.
- [13] M. J. Holman, M. J. Payne, P. Blankley, R. Janssen, and S. Kuindersma. "HelioLinC: A Novel Approach to the Minor Planet Linking Problem". In: *The Astronomical Journal* 156.3, 135 (Sept. 2018), p. 135. DOI: 10.3847/1538-3881/aad69a.

- [14] J. L. Lagrange. “Sur le problème de la détermination des orbites des comètes d’après trois observations. Troisième mémoire”. In: *Nouveaux mémoires de l’Académie royale des sciences et belles-lettres de Berlin* (1783). Reprinted in *Œuvres de Lagrange*, Gauthier-Villars et fils, Paris (1869), volume 4, pp. 496–532.
- [15] P. S. Laplace. “Mémoire sur la détermination des orbites des comètes”. In: *Mémoires de l’Académie royale des sciences de Paris* (1780). Reprinted in *Œuvres complètes de Laplace*, Gauthier-Villars et fils, Paris (1894), volume 10, pp. 93–146.
- [16] A. Milani and G. F. Gronchi. *Theory of Orbit Determination*. Cambridge Univ. Press, 2010.
- [17] A. Milani, M. E. Sansaturio, and S. R. Chesley. “The Asteroid Identification Problem IV: Attributions”. In: *Icarus* 151.2 (June 2001), pp. 150–159. DOI: doi.org/10.1006/icar.2001.6594.
- [18] M. E. Sansaturio and O. Arratia. “Mining knowledge in One Night Stands data sets”. In: *Monthly Notices of the Royal Astronomical Society* 419.4 (Feb. 2012), pp. 3399–3405. DOI: [10.1111/j.1365-2966.2011.19978.x](https://doi.org/10.1111/j.1365-2966.2011.19978.x).
- [19] E. Schunová, M. Granvik, R. Jedicke, G. F. Gronchi, et al. “Searching for the first near-Earth object family”. In: *Icarus* 220.2 (Aug. 2012), pp. 1050–1063. DOI: [10.1016/j.icarus.2012.06.042](https://doi.org/10.1016/j.icarus.2012.06.042).
- [20] R. B. Southworth and G. S. Hawkins. “Statistics of meteor streams”. In: *Smithsonian Contributions to Astrophysics* 7 (Jan. 1963), pp. 261–285.
- [21] L. G. Taff. “On initial orbit determination”. In: *Astronomical Journal* 89 (Sept. 1984), pp. 1426–1428. DOI: [10.1086/113644](https://doi.org/10.1086/113644).
- [22] L. G. Taff and D. L. Hall. “The Use of Angles and Angular Rates I: Initial Orbit Determination”. In: *Celestial Mechanics* 16.4 (Dec. 1977), pp. 481–488. DOI: [10.1007/BF01229289](https://doi.org/10.1007/BF01229289).
- [23] R. Weryk, G. Williams, and R. Wainscoat. “Linking Isolated Tracklets to Improve Asteroid Discovery”. In: *American Astronomical Society Meeting Abstracts #235*. Vol. 235. American Astronomical Society Meeting Abstracts. Jan. 2020, 329.05, p. 329.05.

A Computation of the probabilities associated to the 4-connected subgraphs

We made the assumption that the `link2` solutions are independent in our estimation of the expected number of 4-connected sub-graphs that will be obtained from an observation data set containing $N - 3$ objects where 1 object has 4 tracklets and $N - 4$ objects have only 1 tracklet. This means that we assumed that the probability of linking two tracklets depends only on whether they belong to the same object. Thus, we let p be the probability of linking two tracklets that belong to the same object and we denote by q the probability of linking two tracklets that belong to different objects. The values of p and q as a function of the threshold value of χ_4 are displayed in Figure 34.

Given 4 vertices, there are 38 possible 4-connected graphs as shown in Figure 37. From this figure we can compute the probability p_k to have a 4-connected sub-graph if the tracklets belong to k objects for $k = 1, 2, 3, 4$. Note that, due to our simple assumptions on the data set, the only way to have 4 tracklets belonging to 2 objects is that 3 tracklets belong to one of them. In this way, these

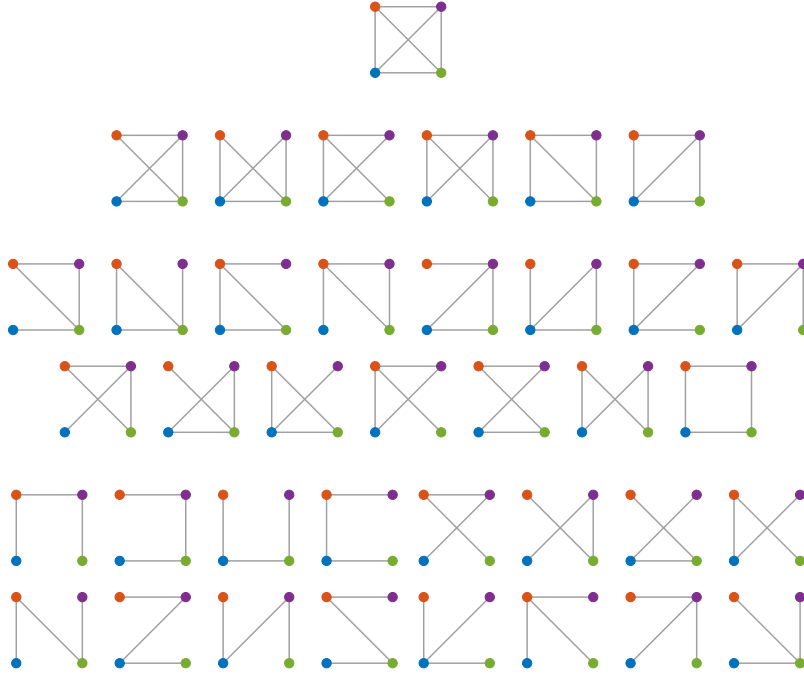


Figure 37: The 38 possible 4-connected graphs.

probabilities are:

$$\begin{aligned}
 p_1 &= p^6 + 6p^5(1-p) + 15p^4(1-p)^2 + 16p^3(1-p)^3, \\
 p_2 &= p^3q^3 + 3p^3q^2(1-q) + 3p^2(1-p)q^3 + 3p^3q(1-q)^2 \\
 &\quad + 9p^2(1-p)q^2(1-q) + 3p(1-p)^2q^3 + (1-p)^3q^3 \\
 &\quad + 6p(1-p)^2q^2(1-q) + 9p^2(1-p)q(1-q)^2, \\
 p_3 &= pq^5 + 5pq^4(1-q) + (1-p)q^5 + 5(1-p)q^4(1-q) \\
 &\quad + 10pq^3(1-q)^2 + 8pq^2(1-q)^3 + 8(1-p)q^3(1-q)^2, \\
 p_4 &= q^6 + 6q^5(1-q) + 15q^4(1-q)^2 + 16q^3(1-q)^3.
 \end{aligned}$$

Finally, formula (9) comes from the property of the binomials

$$\binom{N}{M} = \sum_{k=0}^M \binom{M}{M-k} \binom{N-M}{k},$$

for the particular case of $M = 4$ using the probabilities computed previously:

$$\begin{aligned}
 N_4(\chi_4) &= \binom{4}{4} \binom{N-4}{0} p_1 + \binom{4}{3} \binom{N-4}{1} p_2 + \binom{4}{2} \binom{N-4}{2} p_3 \\
 &\quad + \binom{4}{1} \binom{N-4}{3} p_4 + \binom{4}{0} \binom{N-4}{4} p_4 \\
 &= p_1 + 4(N-4)p_2 + 6 \binom{N-4}{2} p_3 + \left[4 \binom{N-4}{3} + \binom{N-4}{4} \right] p_4.
 \end{aligned}$$